Understanding and modeling tephra transport: lessons learned from the 18 May 1980 eruption of Mount St. Helens

Larry G Mastin, Steven N Carey, Alexa R van Eaton, Julia Eychenne, R S J Sparks

Post-print of the article:
Mastin LG, Carey SN, Van Eaton AR, Eychenne J, Spars RSJ, 2022. Understanding and modeling tephra transport: Lessons learned from the 18 May 1980 eruption of Mount St. Helens. Bull Volcanol 85:4 doi.org/10.1007/s00445-022-01613-0

Understanding and modeling tephra transport: lessons learned from the 18 May 1980 eruption of Mount St. Helens

Larry G. Mastin[1] · **Steven N. Carey**[2] · **Alexa R. Van Eaton**[1] · **Julia Eychenne**[3] · **R. S. J. Sparks**[4]

Abstract
Discoveries made during the 18 May 1980 eruption of Mount St. Helens advanced our understanding of tephra transport and deposition in fundamental ways. The eruption enabled detailed, quantitative observations of downwind cloud movement and particle sedimentation, along with the dynamics of co-pyroclastic-density current (PDC) clouds lofted from ground-hugging currents. The deposit was mapped and sampled over more than 150,000 km^2 within days of the event and remains among the most thoroughly documented tephra deposits in the world. Abundant observations were made possible by the large size of the eruption, its occurrence in good weather during daylight hours, cloud movement over a large, populated continent, and the availability of images from recently deployed satellites. These observations underpinned new, quantitative models for the rise and growth of volcanic plumes, the importance of umbrella clouds in dispersing ash, and the roles of particle aggrega-tion and gravitational instabilities in removing ash from the atmosphere. Exceptional detail in the eruption chronology and deposit characterization helped identify the eruptive phases contributing to deposition in different sectors of the distal deposit. The eruption was the first to significantly impact civil aviation, leading to the earliest documented case of in-flight engine damage. Continued eruptive activity in 1980 also motivated pioneering use of meteorological models to forecast ash-cloud movement. In this paper, we consider the most important discoveries and how they changed the science of tephra transport.

Keywords Mount St. Helens · Tephra · Explosive volcanism · Particle aggregation · Volcanic plume · Umbrella cloud · Ash cloud

Introduction

A defining trend in volcanology since the 1960s has been the shift from qualitative descriptions of volcanic activity to measurement, calculation and ultimately models that forecast how far and how fast tephra moves through the atmosphere, and how severely tephra hazards affect people and property. A search on Google Scholar, for example, for papers containing all the words "volcanic ash," "deposit," and "numerical model" between 1900 and 1960 returns no results. The same search with end dates of 1970, 1979, 1990, and 2000 will return 3, 26, 102, and 290, respectively. This rate of increase is several times faster than the fifteen-year doubling time of scientific publications overall (Larsen and von Ins 2010), reflecting an evolution from narrative description of phenomena to physics-based conceptual models and quantitative numerical models. In the science of tephra transport, the numbers increased dramatically around the time of the 1980 Mount St. Helens eruption.

The Mount St. Helens eruption occurred at a time of rapid advance in understanding of tephra transport and deposition. By the 1970s, tephra specialists began to integrate field-based observations with the physics of plume rise and particle settling. For example, Walker et al. (1971) experimentally measured the fall velocity of pyroclasts, while Wilson

✉ Larry G. Mastin
lgmastin@usgs.gov

[1] U.S. Geological Survey, David A. Johnston Cascades Volcano Observatory, Vancouver, WA 98683, USA

[2] Graduate School of Oceanography, University of Rhode Island, Kingston, USA

[3] Département Des Sciences de La Terre, Université Clermont Auvergne, Clermont-Ferrand, France

[4] School of Earth Sciences, University of Bristol, Bristol, UK

(1972) calculated particle trajectories in the atmosphere. Observations from Heimaey and Stromboli in 1973 showed that debris was ejected upward through a gas thrust region (Blackburn et al. 1976; Sparks and Wilson 1976; Wilson 1976), where it slowed due to drag and negative buoyancy, but then accelerated into a much higher convective thrust region if enough air could be entrained to make the mixture buoyant. With insufficient entrainment, the column would collapse, providing a mechanism for ignimbrite formation. Sparks and Wilson (1976) found that column collapse was favored by eroding vent walls, reducing magmatic gas content, or reducing exit velocity. They developed a pioneering model of Plinian column variations with height and used it to calculate particle trajectories by adapting established fluid dynamical models of plumes and jets. If plumes attain buoyancy, buoyant plume theory (Morton et al., 1956) suggested that $H \propto \mathrm{MER}^{1/4}$, where H is plume height and MER is mass eruption rate. This relationship was confirmed by observations of well-documented eruptions (Settle 1978; Wilson et al. 1978).

Thus, the 1970s brought a new fundamental understanding of explosive eruption dynamics which set the stage for quantitative transport modeling. However, a large, well-observed eruption where ideas could be tested was needed.

May 18: overview and key observations

By 1980, thanks to field studies in the previous 1–2 decades, Mount St. Helens was known to be the most active and explosive volcano in North America's Cascade Range. In the late 1950s, volcanologists from the U.S. Geological Survey (USGS) began a systematic study of the eruptive history of Cascade volcanoes (Crandell and Waldron 1956; Crandell et al. 1962; Crandell 1963). Work started at Mount Rainier, which was assumed to be the most hazardous; but by the mid-1970s, investigators recognized that Mount St. Helens had produced more explosive, tephra-forming eruptions with more Holocene tephras than any other Cascade volcano, including three large deposits (>0.1 km^3) since the 1400s C.E. (Crandell and Mullineaux 1978).

Volcanologists were therefore not surprised when Mount St. Helens awakened in 1980 (Christiansen and Peterson 1981; Foxworthy and Hill 1982). Following two months of inflation, a M 5.2 earthquake at 08:32:11 Pacific Daylight Time (PDT = UTC-7: all times in this paper are local, 24-h time) on 18 May 1980 (Fig. 1). The earthquake caused the north flank to slide away in the largest subaerial landslide yet documented, uncorking a pressurized cryptodome that expanded north as a lateral blast, and then rose buoyantly to > 30 km above sea level (asl) as an umbrella cloud (Fig. 2), dropping branches, mud rain, and accretionary lapilli on nearby eyewitnesses (Waitt 2014). At the summit, a vertical eruptive column rose to about 14 km asl shortly after 09:00 and fluctuated between 14 and 19 km asl until about 17:00 before subsiding (Fig. 1). The east-moving ash cloud (Fig. 3a) crossed the Idaho border (400 km downwind) by noon, the west edge of Yellowstone National Park (1000 km) by about 17:30, and continued towards the East Coast of the U.S. Impacts on the ground (Damby et al. (this volume)) included road closures (Schuster 1981), respiratory problems (Baxter

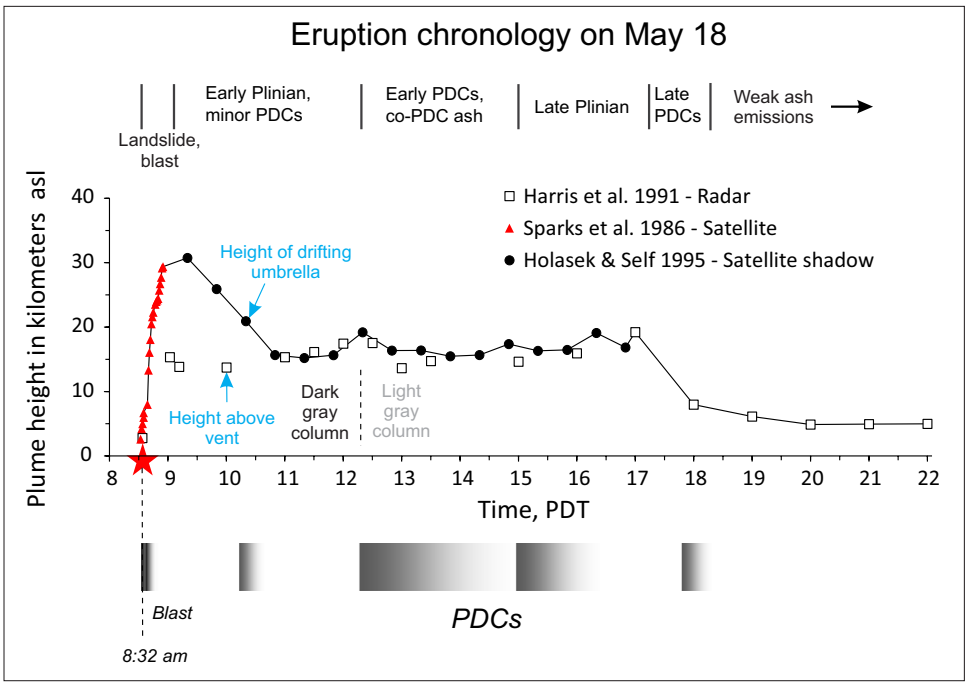

Fig. 1 (a) Chronology of eruptive activity on 18 May 1980, including plume height with time, and time of occurrence of PDCs. Radar heights reported by Harris et al. (1981) are "near the volcano" and likely to reflect column heights above the vent, whereas satellite cloud-top heights reported by Holasek and Self (1995) are not restricted to the vent area. During the morning of 18 May, the data from Holasek and Self (1995) likely reflect the height of the drifting umbrella cloud

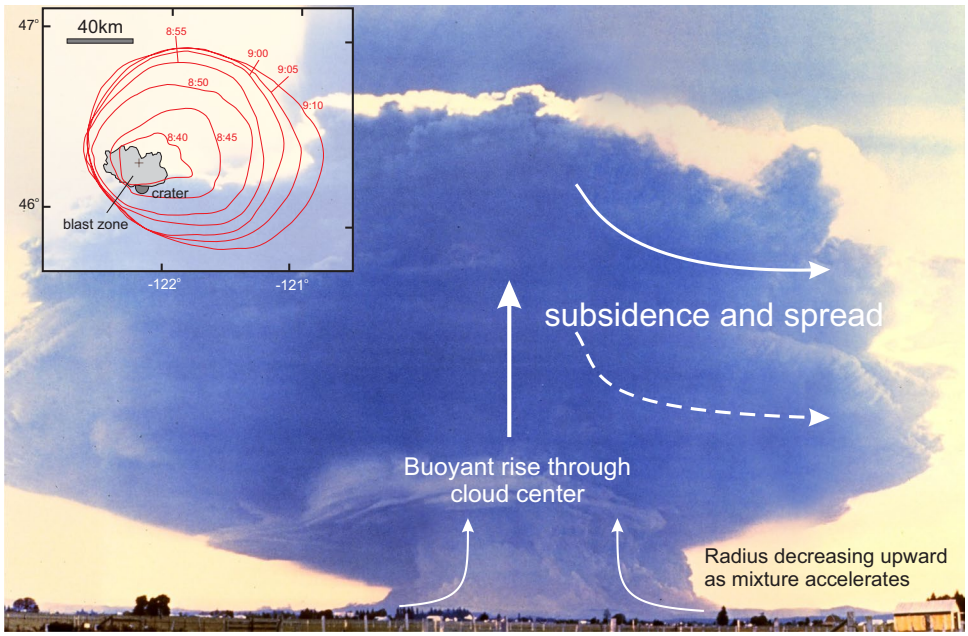

Fig. 2 Photomosaic of the growing Mount St. Helens umbrella cloud, taken by Rocky Kolberg from about 3.2 km NNE of downtown Toledo, Washington, USA (46.4686°N, – 122.8413°W), at about 08:52. Annotations indicate key processes inferred. Inset shows successive outlines of the growing umbrella cloud, taken at 5-min intervals from 08:40 to 09:10, from a military satellite as reported in Sparks et al. (1986, Fig. 8). Wikimedia Commons photo (https://commons.wikimedia.org/wiki/File:MtStHelens_Mushroom_Cloud.jpg)

et al. 1983; Bernstein et al. 1986), aircraft evacuations at Fairchild Air Force Base near Spokane, discharging of raw sewage into the Yakima River when ash clogged treatment filters (Day and Fisher 1980), and damage to agricultural machinery and crops (Cook et al. 1981).

At least three factors made this event a milestone in volcanology. One was the direct observation of phenomena such as the lateral blast. Second, emerging technology led to dramatic improvements in satellite imagery (Menzel 2020) with unprecedented temporal and spatial resolution, enabling tracking of the volcanic plume (Harris et al. 1981). A third factor was clear weather. The eruption occurred on a Sunday in view of thousands of cameras and produced a deposit that fell over land, in an area where tephra could be quickly accessed and sampled before significant modification by wind and rain.

The 1980 Mount St. Helens eruption attracted scientists from around the globe. The data have been mined for decades for insights into the nature of ash hazards. The timing of the event, occurring when computer technology and ash transport calculations were nascent, jump-started the field of ash-transport modeling, which is now an operational mainstay of ash-hazards forecasting.

What we learned

An immense amount was quickly learned in the days and weeks after May 18 through vivid images, but it took many years to develop a fuller picture. Some of the most lasting discoveries are highlighted below.

Insights from satellite, radar, photographs, and eyewitness accounts

The lateral blast and blast co-pyroclastic-density–current (co-PDC) plume

Ground-based photos were integrated with other observations to develop a detailed picture of the sequence of events (Fig. 1) (Voight 1981; Moore and Rice 1984; Pierson 1985; Sparks et al. 1986; Hoblitt 2000). Photo reconstruction showed that the north flank slid away as three separate blocks (Moore and Albee 1981). The lateral blast and plumes rising from it may have developed from two explosions (Moore and Rice 1984; Hoblitt 2000). From satellite and photo reanalysis, the first explosion, "cloud I," began as the mountain's north flank slid away, about a half minute after the M 5.2 earthquake (Voight 1981). The second, "cloud II," began at 1.5 min (Moore and Rice 1984), was manifested by intense infrared radiation in satellite images, and ascended into the atmosphere at speeds up to 70 m/s, centered on a location 12–14 km north of the volcano. Moore and Rice (1984) attributed the second explosion to collision of blast/avalanche with Johnston Ridge or perhaps steam generation in the North Fork Toutle River Valley. Hoblitt (2000) suggested that explosion 2 began with detachment of slide block II and that the cloud "exploded" when reaching rugged terrain north of the North Fork Toutle River. Clouds I and II reached about 7 km altitude.

Ascent of the blast co-PDC plume

Multiple satellite imagery sources, including restricted national sources and ground-based photos, were combined to

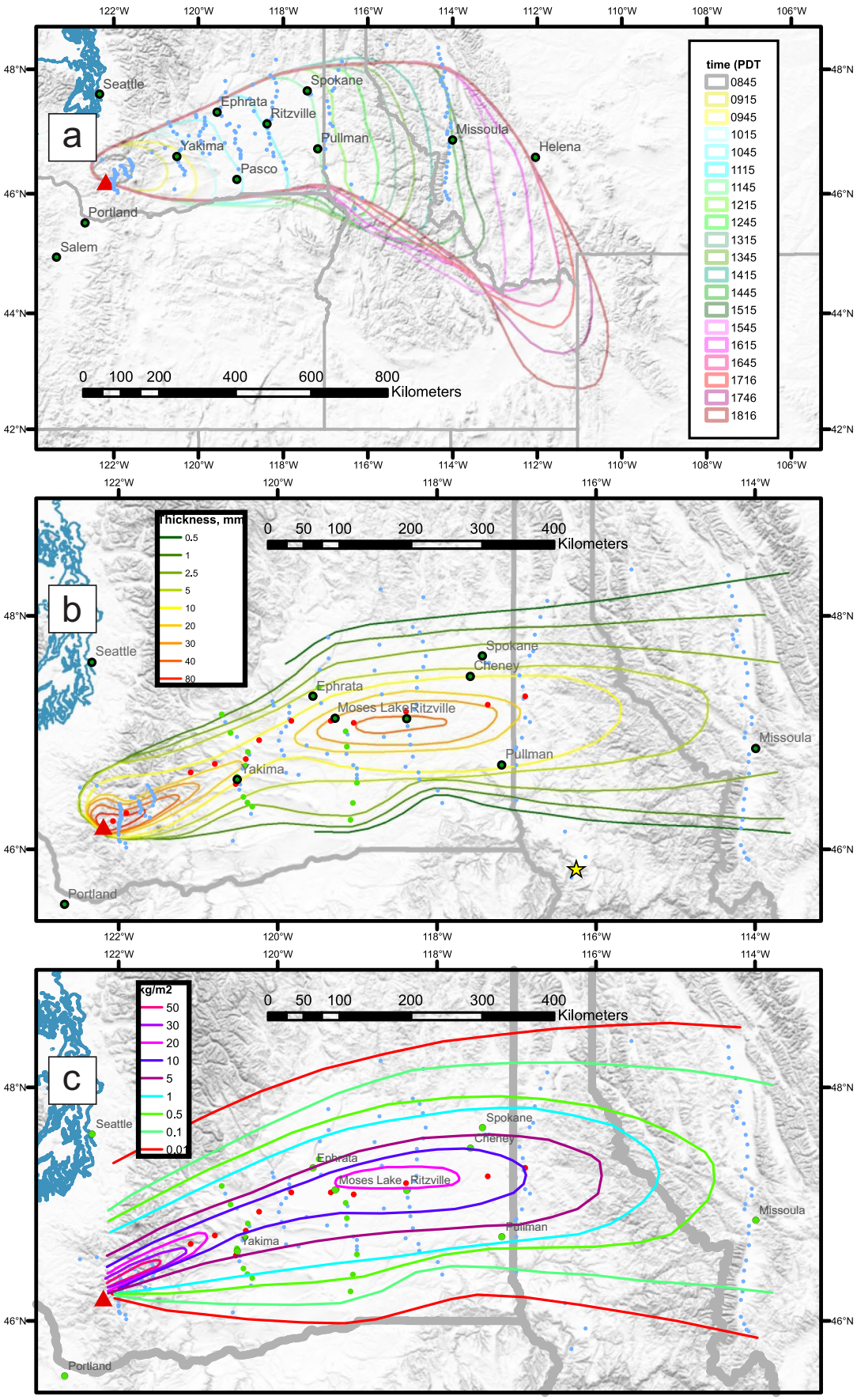
a
b
c
Seattle
Portland
Salem
Spokane
Ephrata
Ritzville
Pullman
Yakima
Pasco
Missoula
Helena
Cheney
Moses Lake
time (PDT
0845
0915
0945
1015
1045
1115
1145
1215
1245
1315
1345
1415
1445
1515
1545
1615
1645
1716
1746
1816
Thickness, mm
0.5
1
2.5
5
10
20
30
40
80
kg/m2
50
30
20
10
5
1
0.5
0.1
0.01
0 100 200 400 600 800
Kilometers
0 50 100 200 300 400
Kilometers
122°W
120°W
118°W
116°W
114°W
112°W
110°W
108°W
106°W
48°N
46°N
44°N
42°N

◂**Fig. 3** (a) Map showing outlines of the ash cloud at different times on 18 May from Sarna-Wojcicki et al. (1981, Fig. 332); (b) isopach map of the deposit (mm), from Sarna-Wojcicki et al. (1981, Fig. 336); (c) isomass map of the deposit (kg/m^2), from Sarna-Wojcicki et al. (1981, Fig. 338). Blue circles represent sample locations (Durant et al. 2009). Red triangle gives location of Mount St. Helens. Red dots in (b) and (c) give sample locations in Figs. 6a, b, d (Carey and Sigurdsson 1982). Green dots in (b) and (c) give sample locations in Fig. 7. Yellow star in (b) gives the location of aggregates photographed in Fig. 5

give a detailed picture of the transition from lateral blast—a horizontally directed expulsion of pyroclastic currents—to a vertically rising plume (Moore and Rice 1984; Sparks et al. 1986). The data from two classified U.S. Air Force infrared geostationary satellites (Rice 1981; Sparks et al. 1986) allowed rates of plume rise and umbrella expansion to be quantified with a time resolution of 5 min. These observations provided the first direct documentation of the buoyant liftoff process now recognized as a key aspect of co-PDC plumes.

These data showed that pyroclastic density currents from the blast expanded until about 08:36:00–08:37:30. Toward its outer edges, an overriding current of gas and particles began to separate from a dense, granular undercurrent (Gardner et al. 2017) while passing over ridges, leaving patches of standing trees before rejoining the main flow. Toward the center of the blast zone (the area where trees were toppled), a buoyant cloud began to rise. Shortly after lifting off, the ground-hugging PDC slowed its outward lateral movement and stalled. A photomosaic (Fig. 2) illustrates the rising plume at about 08:52, with a radius in the lowermost kilometer that decreases as air is drawn in and then spreads out at multiple levels at higher altitude. Satellite data (Sparks et al. 1986) showed ascent velocities up to 110 m/s. The plume reached a height of 25 km by 08:50 and then 31 km by about 08:54 following a late pulse. In map view, the radial growth of the umbrella cloud averaged 20–25 m/s between 08:50 and 09:10, and the westward side of the cloud pushed upwind 28 km until it stagnated as the radial expansion speed approached that of the ambient winds. Negatively buoyant material from the top of the plume collapsed into the neutrally buoyant umbrella with increased crosswind spreading and downwind dispersal (Bursik et al. 1992a; Holasek and Self 1995).

Physics of plume rise and spreading The dynamics of this cloud were clearly different from that of a steady Plinian column, which exits the vent as a negatively buoyant high-speed jet, decelerates, and then accelerates again after attaining buoyancy (Sparks and Wilson 1976). In contrast, this co-PDC cloud from Mount St. Helens lifted off the ground as a positively buoyant thermal with little initial upward velocity. Buoyant liftoff from a ground-hugging PDC is attributed to reversal of buoyancy with respect to the overlying atmosphere by a combination of sedimentation, entrainment, and heating of entrained air (Sparks et al. 1986; Woods and Wohletz 1991; Gardner et al. 2017). The PDC decelerates rapidly and motion transitions from lateral to vertical. Buoyant liftoff was also demonstrated in PDCs from explosive activity later in the day on May 18 (Figs. 1, 4d) and during later eruptions in 1980 (Calder et al. 1997), though not with the same intensity as from the lateral blast.

On reaching the height of neutral buoyancy in the atmosphere, both vent-derived and co-PDC plumes may spread radially as an umbrella cloud. A theoretical treatment of these two phenomena (Sparks et al. 1997, Ch. 11) found that umbrella clouds rising from sustained sources should grow at about $R \propto t^{2/3}$ (Sparks et al. 1997, Eq. 11.8), whereas those rising from instantaneous sources like the Mount St. Helens blast cloud should grow at $R \propto t^{1/3}$ (R = cloud radius, t = time). Observed umbrella growth rates at Pinatubo, Philippines, in 1991 follow the predictions for a steady plume (Holasek et al. 1996). The Mount St. Helens co-PDC plume fell between that of a steady and an instantaneous plume, reflecting perhaps that it was fed over a period of time comparable to the rise time (Woods and Wohletz 1991; Sparks et al. 1997).

Plinian phase and downwind plume spreading

USGS personnel made continuous airborne observations for more than 4.5 h (Krimmel and Post, 1981). From about 09:00 until 12:15, eyewitnesses and radio logs (Criswell 1987) indicate that a steady Plinian column rose from the vent to 14–19 km asl (Figs. 1, 4c) (Christiansen and Peterson 1981; Criswell 1987; Holasek and Self 1995). Shortly after noon, lighter-toned material appeared discontinuously from the vent, eventually composing most of the column; then about 12:15, eruptive vigor increased and PDCs started to pour northward through the crater breach (Foxworthy and Hill 1982; Criswell 1987). An elongate ash plume from above the PDCs extended northeast, rising to more than 14 km asl (Harris et al. 1981; Holasek and Self 1995). From 13:30 to 15:00, PDCs erupted more episodically and then eventually abated by ~ 16:25, after which the Plinian plume reached its greatest height of ~ 19 km asl, before starting to decline around 17:30.

Through a combination of eyewitness accounts, good timing, and new technology, we learned a great deal about the phenomena that dispersed tephra. The U.S. National Weather Service (NWS) tracked plume height and downwind movement continuously from radars in Portland, Seattle, and Spokane (Harris et al. 1981). In addition, the cloud was imaged every half hour, in both visible and thermal infrared (10–12 μm) (Holasek and Self 1995) by the GOES-3 satellite.

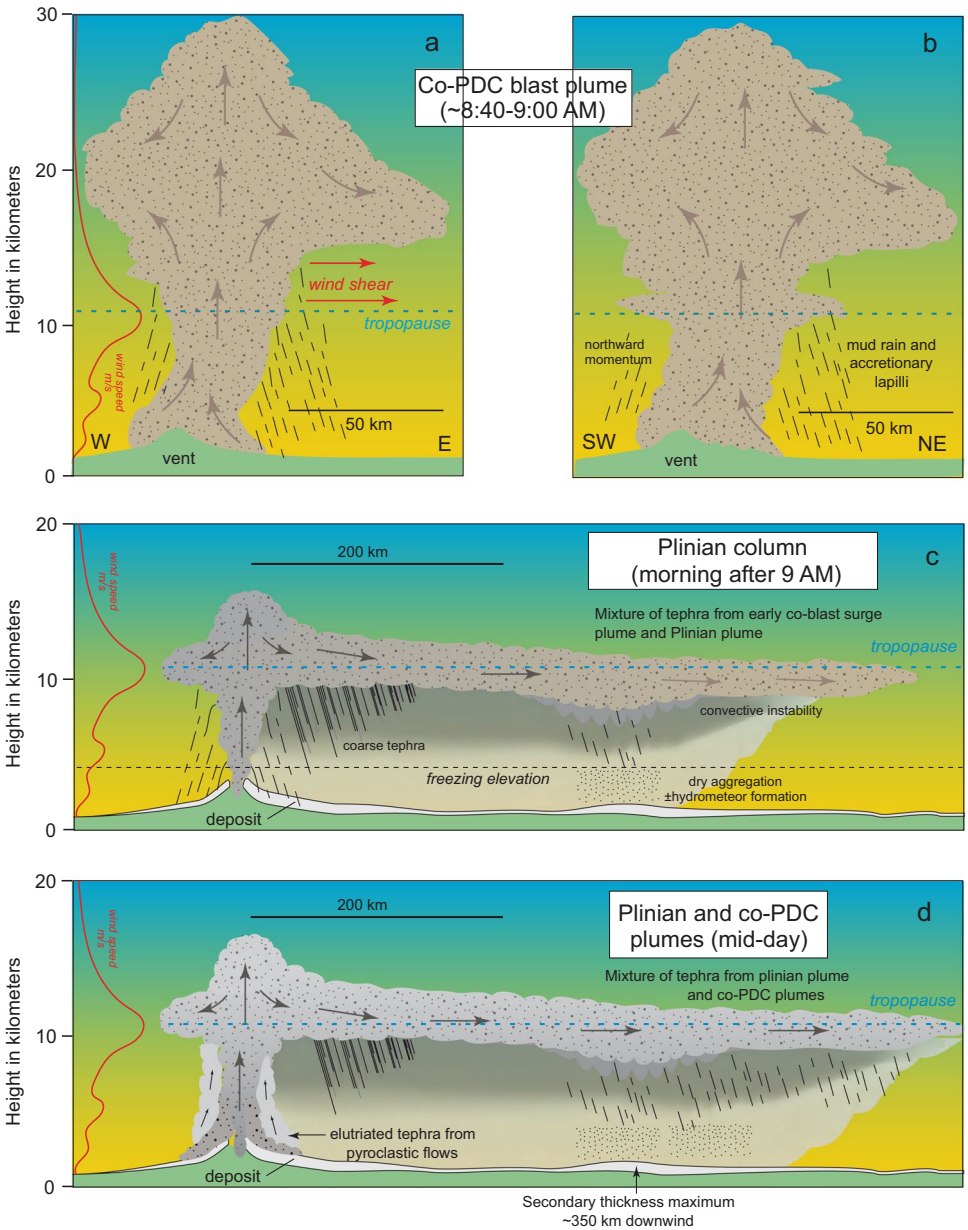

Fig. 4 Key processes and features of the plume and downwind cloud at three times on 18 May 1980 eruption. (a, b) Rise and expansion of the coignimbrite plume, 08:40–09:00 local time. (c) Movement of the downwind cloud shortly before noon, as it was being fed by a Plinian column from the vent. (d) Downwind movement of the cloud in late afternoon, as it was being fed by ash from both the Plinian column and from ash elutriating from PDCs near the vent. Some of the key processes described in this paper are labeled

Modern techniques to identify ash clouds in infrared imagery (e.g., Prata 1989) had not yet been developed, and remote sensing analysts could track ash only during daylight hours based on grayscale tones in visible imagery. In GOES-3 visible imagery, the cloud moved eastward at about 100 km/h in the first 1000 km before night fell (Fig. 3a). The following day, the center of the increasingly diffuse cloud passed over the mid-continent, New England, maritime provinces of Canada, and into the North Atlantic (Sarna-Wojcicki et al. 1981). At downwind locations, the ash cloud arrived overhead before it started depositing at ground level (Durant et al. 2009; Eychenne et al. 2015) (Figs. 4c, 5). At Spokane, for example, the delay was about 1.75 h (Sarna-Wojcicki et al. 1981; Durant et al. 2009).

Over years of post-eruption analysis, the scientific community learned many things about the factors controlling ash cloud transport. Some key findings are listed below and illustrated in Fig. 4:

- Relationships between plume height and eruption rate generally followed established height-rate relationships at the time (Settle 1978; Wilson et al. 1978), but showed new complexities. Carey et al. (1990) found that the mass eruption rate inferred from deposit mass was a few times greater than predicted by plume height. The discrepancy was attributed either to partitioning of the erupted mass into PDCs (e.g., Carey et al. 1990) or bending of the plume by high winds (Degruyter and Bonadonna 2012).

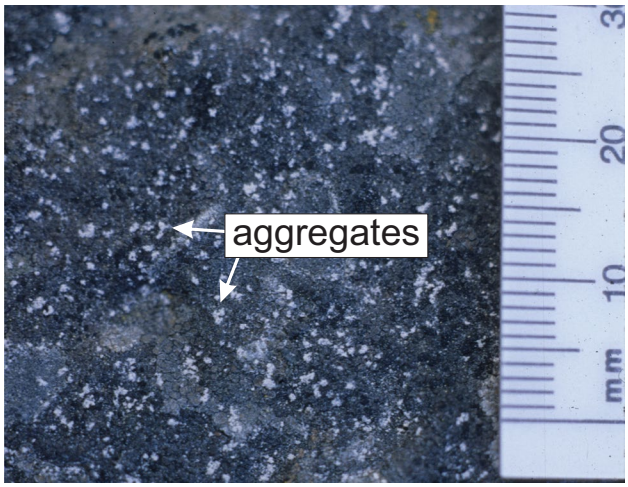

Fig. 5 Ash aggregates on pavement, photographed by Spencer Wood on the morning of May 19, 1980, on Whitebird Grade near Grangeville, Idaho (45.8289°N, 116.2465°W), 470 km ESE of Mount St. Helens. Location given by yellow star in Fig. 3b

The addition of Mount St. Helens data into later compilations of eruption rate and plume height (e.g., Sparks et al. 1997; Mastin et al. 2009; Aubry et al. 2021) broadened the scatter and added to growing recognition of complexity.

- Both the initial umbrella cloud and later Plinian column were undercooled by about 15 °C (meaning the cloud top was colder than the atmosphere at that height) due to adiabatic expansion during plume ascent (Holasek and Self 1995). The cloud equilibrated with surrounding temperatures over about 30–60 min. Undercooling is now a commonly recognized phenomenon in stratospheric eruptions (e.g., Woods and Self 1992; Holasek et al. 1996) and quantified in many plume models (e.g., Woods and Self 1992; Suzuki et al. 2016). Undercooling complicates efforts to estimate stratospheric cloud height based on cloud-top temperature. Holasek and Self (1995) overcame this complication by pioneering the use of cloud geometry to estimate plume height.
- Although plume-top heights ranged from ~ 14 to 31 km, the distal cloud moved eastward at much lower levels, about 10–14 km asl, where the cloud was neutrally buoyant and wind speeds were the highest (Sarna-Wojcicki et al. 1981; Woods et al. 1995) (Fig. 4c). It is now recognized that ash dispersal tends to occur at altitudes well below the overshooting top height (e.g., Holasek et al. 1996).
- Over distances of several hundred kilometers downwind, the width in plan view of the May 18 ash cloud increased with the square root of distance, suggesting that gravity current spreading was a more important cloud-widening process than turbulent diffusion (Bursik et al. 1992a). This finding contradicts assumptions that cloud widening results primarily from turbulent diffusion (e.g., Folch 2012). The detailed observations of Holasek and Self (1995) were also used by Bonadonna and Phillips (2003) to quantify for the first time the relative effects of gravitational spreading and wind advection on plume widening and downwind transport.
- Gravitational instabilities at the base of the downwind cloud formed mammatus structures a few hundred kilometers downwind (Fig. 4c). Also, a region of high radar reflectivity appeared at a few hundred kilometers downwind, at about 2–3 h after the eruption start, and persisted for about 11 h (Harris et al. 1981; Durant et al. 2009). This high-reflectivity zone was interpreted by Durant et al. (2009) to result either from the growth of aggregates in the cloud or from frozen hydrometeors falling through the melting level to form liquid water. The downwind distance, about 300 km, coincides with the location of a secondary thickness maximum described below (Fig. 4d).

Insights from the fall deposits

The 18 May 1980 eruption produced a widespread tephra-fall deposit distributed over 150,000 km^2 with a total volume of about 0.25 km^3 DRE (dense rock equivalent, Sarna-Wojcicki et al. (1981)). Fallout occurred east of the volcano in the states of Washington, Idaho, and Montana (Folsom and Quinn 1980; Sarna-Wojcicki et al. 1981; Carey and Sigurdsson 1982), although some fine ash was transported to the west and northwest at high levels in the atmosphere (Danielsen 1981). Volcanologists were able to sample and map out the distribution of a pristine fallout deposit prior to significant erosion and reworking. Observations of eruption column height (Harris et al. 1981), atmospheric trajectories (Rosenfeld 1980; Danielsen 1981), eruption chronology (Christiansen and Peterson 1981; Criswell 1987), and eyewitness accounts (Rosenbaum and Waitt 1981) enabled quantitative assessment of factors controlling the formation of widespread tephra-fall deposits from a major explosive eruption. Additionally, the rich diversity of observations and complete documentation made this a benchmark event for subsequent studies and refinements of models for atmospheric dispersal of tephra (e.g., Armienti et al. 1988; Fero et al. 2008; Folch et al. 2010; Mastin et al. 2016).

Questions remain about the footprint of the ash deposit. Existing maps are not entirely consistent with each other (e.g., Folsom and Quinn 1980; Sarna-Wojcicki et al. 1980) and later observations noted ashfall in new places (Jensen et al. 2019b). Jensen et al. (2019a, unpublished data) examined archival news reports and eyewitness observations that suggest that thicknesses of 0.5–1 mm extended well into southeastern British Columbia and southern Alberta. There

are credible accounts of ash "dustings" much farther north, in Edmonton, Saskatchewan, and the U.S. east coast (Tilling 1984; S. Moran, USGS, pers. commun. 2022). Cutler et al. (2020) revisited the May 18 tephra deposit and found good preservation where the original thickness exceeded 0.5 cm. Related studies performed decades after 1980 showed that winnowing of fine ash with time could modestly reduce fine-ash content (Cutler et al. 2021) and that the quality of preservation depends on surface vegetation and development of biocrusts (Cutler et al. 2018).

Downwind and crosswind sedimentological variations

Detailed measurements of the 18 May 1980 tephra fall distribution included both thickness and mass per unit area (Figs. 3b,c) (Folsom and Quinn 1980; Sarna-Wojcicki et al. 1980; Carey and Sigurdsson 1982), making this at the time the most thoroughly documented fall deposit out to its distal limits. Most previous studies lacked data on distal tephra. By combining mass loading and thickness measurements, investigators calculated bulk deposit density values ranging from > 1000 kg/m^3 in proximal areas to < 100 kg/m^3 distally (Fig. 6c) (Folsom and Quinn 1980; Sarna-Wojcicki et al. 1980). Several distinct layers were identified at most sites, which represented tephra from the initial co-PDC blast cloud, the main Plinian column, and secondary plumes generated by PDC generation (Sarna-Wojcicki et al. 1981). A distinctive feature of the deposit is the occurrence of a secondary thickness maximum approximately 325 km east of Mount St. Helens in the vicinity of Ritzville, Washington (Figs. 3b, 4c,d). This feature had been documented in only a few other fall deposits, most notably associated with the 1932 explosive eruption of Quizapu volcano, Chile (Hildreth and Drake 1992), but its significance had not been examined in detail.

The May 18 tephra fall deposit consisted of a mixture of pumice, glass shards, accidental lithics, and crystals of plagioclase, orthopyroxene, amphibole, sparse clinopyroxene, and Fe-Ti oxides sourced from the primary dacitic magma, cryptodome, and older volcanic deposits of Mount St. Helens. These components varied systematically downwind along the main dispersal axis, controlled by the density and size of individual components (Carey and Sigurdsson, 1982). The dominantly dacitic magma erupted on May 18 consisted of about 70% rhyodacitic melt and 30% pheno- and microphenocrysts (Blundy and Cashman 2001) (Rutherford et al. 1985) (Kuntz et al. 1981). The deposit consisted largely of pumice and lithics out to about 50 km (Carey and Sigurdsson, 1982). With increasing distance from source, the percentage of crystals and glass shards increased significantly, with crystal content reaching a peak between about 150 and 200 km distance (Fig. 6d). At 175 km from source, the fall deposit was highly enriched in crystals of plagioclase and mafic phases, resembling beach sand. In the area of the secondary thickness maximum, the deposit was dominated by fine, glassy tephra. SEM imaging (Eychenne et al. 2015) and glass geochemistry (Cutler et al. 2020; Foo et al. 2020) discriminated components from the initial blast co-PDC cloud (fragments of dense cryptodome and older, altered volcanic deposits, higher glass SiO_2) and more vesicular magma from the later Plinian phase and associated PDCs. Surprisingly, beyond 150 km from vent, about half of the tephra by mass was derived from the initial co-PDC blast cloud even though that blast phase was much shorter than the later Plinian and PDC activity. These high-resolution componentry analyses demonstrated that significant lateral facies variations can occur in fall deposits from multi-phase eruptions.

As with other tephra-fall deposits, the grain size of the May 18 sequence decreased regularly with distance from source (Fisher and Schmincke 1984), but displayed a distinct bimodal character in the bulk deposit and within individual stratigraphic units (Fig. 6a) (Carey and Sigurdsson 1982; Durant et al. 2009; Eychenne et al. 2015). A coarse mode became systematically finer with increasing distance from source, whereas a fine mode remained relatively constant (Fig. 6b). At about 400 km from source, the grain size became unimodal (Fig. 6a). Subsequent work with more samples quantified the different modes and their areal distribution downwind and crosswind (Eychenne et al. 2015). Transects perpendicular to the main dispersal axis (Fig. 7) showed the fine ash increasing in proportion to the north and the coarse mode increasing to the south (Eychenne et al. 2015). The fine-ash mode is mostly attributable to the initial blast co-PDC cloud. This work demonstrated that the deposit was derived from at least two distinct plumes, initially at different altitudes, that eventually merged downwind. The initial blast co-PDC plume was injected to a height of > 30 km asl and was displaced to the north of Mount St. Helens, whereas the second, longer-lived plume was generated from a Plinian column and co-PDC clouds rising mostly over the summit and attaining heights of about 14–19 km asl (Harris et al. 1981).

Proximal ash aggregation

Ash aggregation occurred within the May 18 ash plumes in distinct ways depending on the phase of the eruption and distance from source. Accretionary lapilli ranging from a few millimeters to about 1 cm in diameter (Fig. 8a) are preserved in the proximal deposits of the initial blast co-PDC plume. Eyewitnesses described falling mudballs by about 09:00 which variably felt "ice cold" or "a little warm" to the touch (Rosenbaum and Waitt 1981). Some mudballs, about 1 cm in size, splatted on car windshields. Sisson (1995) produced isopleth maps of ash aggregate diameters (Fig. 8a) and concluded that proximal sedimentation from

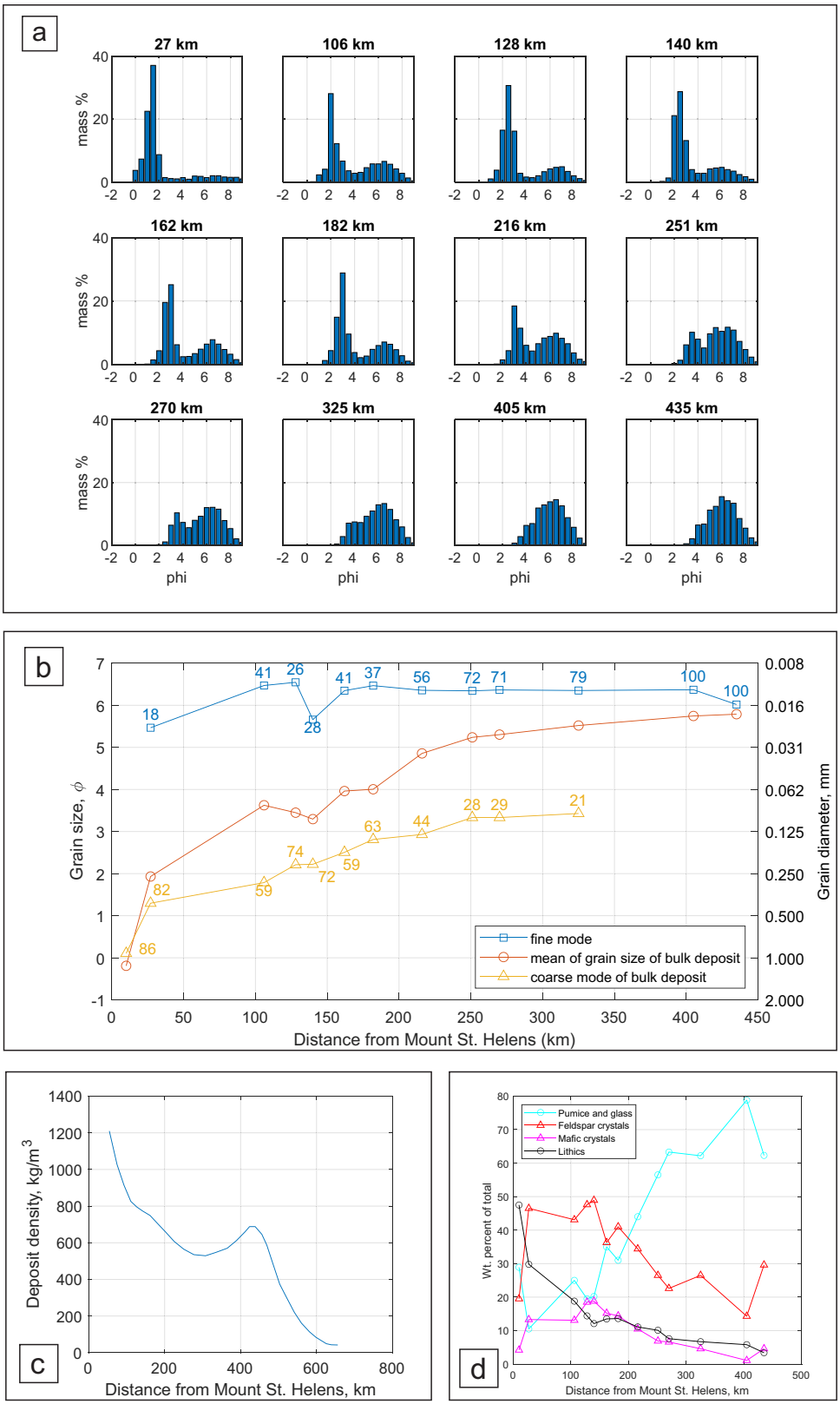

Fig. 6 (a) Grain-size distribution of the bulk fall deposit at different distances downwind along the main dispersal axis. Data from Carey and Sigurdsson (1982) (Fig. 3). (b) Plot of the size of the coarse mode, fine mode, and mean grain size of the bulk fall deposit as a function of distance downwind. Numbers on the blue and yellow curves indicate the weight percent of the total deposit that each mode represents at various distances downwind. After Carey and Sigurdsson (1982). (c) Bulk deposit density versus distance downwind from Mount St. Helens. After Sarna-Wojcicki et al. (1981). (d) Variations in componentry with distance. Data from Carey and Sigurdsson (1982) (Fig. 7). Sample locations given as red dots in Figs. 3b, c. Data used in Figs. 6a, b, d provided in Table S1

the giant umbrella cloud was dominated by wet aggregation, although the origin of the water remains enigmatic. Magmatic water comprised only a few weight percent of the cryptodome magma, and the eruption occurred on a clear, dry day, limiting the amount of moisture entrainment from the surrounding atmosphere. External water could have been

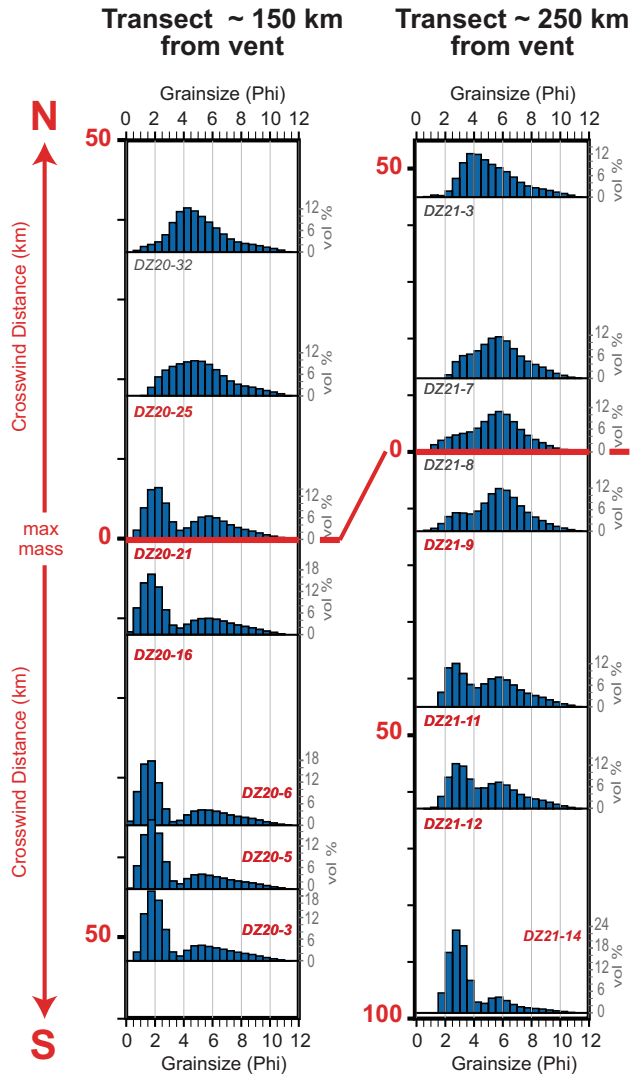

Fig. 7 Grain-size distributions along north–south transects across the deposit in central Washington. sample locations given as green dots in Figs. 3b, c. Data from Durant et al. (2009)

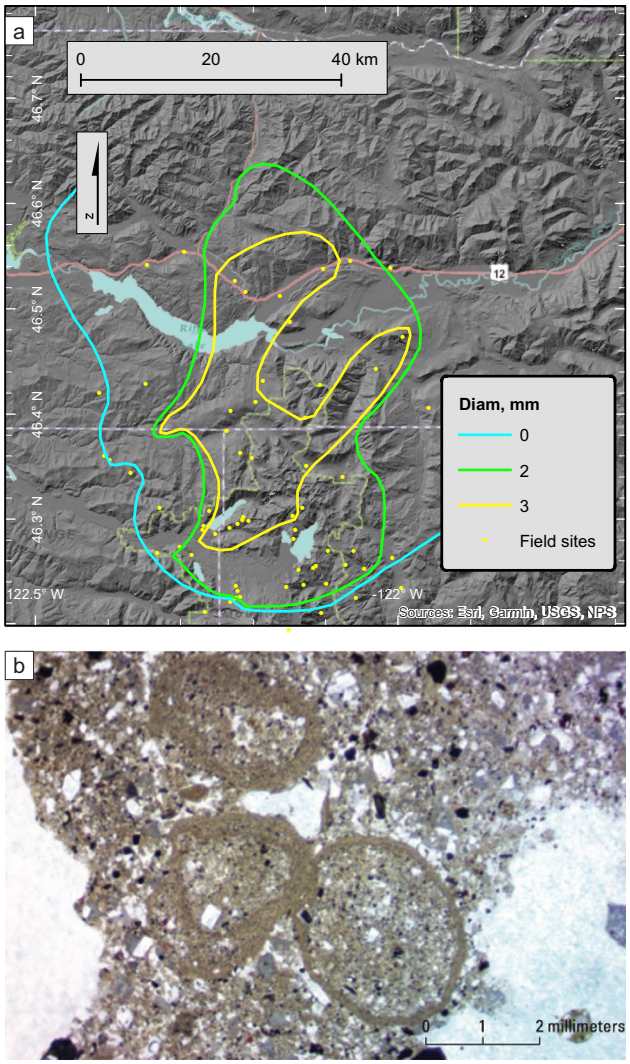

Fig. 8 (a) Isopleth map of diameter of aggregates in the blast ashfall deposit. From Sisson (1995). (b) Thin section of accretionary lapilli collected from the blast ashfall. Photo by Alexa Van Eaton

sourced from the hydrothermal system within the saturated edifice and glaciers/snowpack pulverized by the landslide (Sparks et al. 1986; Hoblitt 2000). These other sources of water increased the moisture content of the fragmenting cryptodome, portions of the blast surge, and the stratospheric co-PDC blast plume.

Other phases of the May 18 eruption contain evidence for aggregation on a smaller scale. Unit C1 of Waitt and Dzurisin (1981) represents deposits up to 80 km distant, derived from co-PDC clouds on the afternoon of May 18. The ash contains concentrically structured, millimeter-scale accretionary lapilli, which are only present near the margins of Spirit Lake (Fig. 8b). Waitt and Dzurisin (1981) proposed that aggregation only took place when the PDCs entrained moisture as they swept across Spirit Lake. These contrasting observations of pervasive, wet aggregation in the blast co-PDC ashfall and localized aggregation within the afternoon PDC's have influenced interpretations of the roles of external moisture on ash transport and fallout in other deposits worldwide (e.g., Oruanui (Van Eaton and Wilson 2013) and Tenerife (Brown et al. 2009)). Aggregation processes also occurred in the downwind, distal cloud, as described below.

Secondary thickness maximum and enhanced fine ash sedimentation

Early simulations of the May 18 tephra fall using a simple particle trajectory model investigated the origin of the second thickness maximum in western Washington (Carey and

Sigurdsson 1982). Modeling inputs included (1) the proportions of different components, their sizes, densities, and settling velocities; (2) transport elevations, plume spreading, and wind velocities; and (3) estimates of total source grain-size distribution. The results demonstrated that the second thickness maximum could not be reproduced if deposition was controlled by fallout of particles individually. Fine ash (< 63 microns) in the second thickness maximum area should have been transported much farther based on their settling velocities, wind strength, and elevation of transport. They concluded that formation of a second thickness maximum could only be generated if fine ash had formed aggregates and settled at a higher velocity than their constituent particles (Fig. 9a). Support for this inference came from the collection of loosely bound aggregates ("Sorem clusters") in Pullman, Washington, 390 km east of Mount St. Helens (Sorem 1982). Aggregates were typically 500–250 microns in diameter, consisted predominantly of glass shards with some crystals, and were likely held together by a combination of mechanical interlocking and/or electrostatic attraction (Sorem 1982).

Dry aggregation alone cannot explain all the features of fine ash from the May 18 fall deposit, especially the proximal fine-ash deposition and the consistency of the fine-mode size over large horizontal distances. Consequently, enhanced fallout of fine ash is thought to be the combined result of dry and wet aggregation; detrainment instabilities of cloud base; hydrometeor formation, settling, and destruction; and entrainment of small particles by larger ones (Fig. 4d) (Durant et al. 2009; Eychenne et al. 2015).

Recognition of fine-ash aggregation at Mount St. Helens has implications for tephra-fall hazards. Premature fallout of

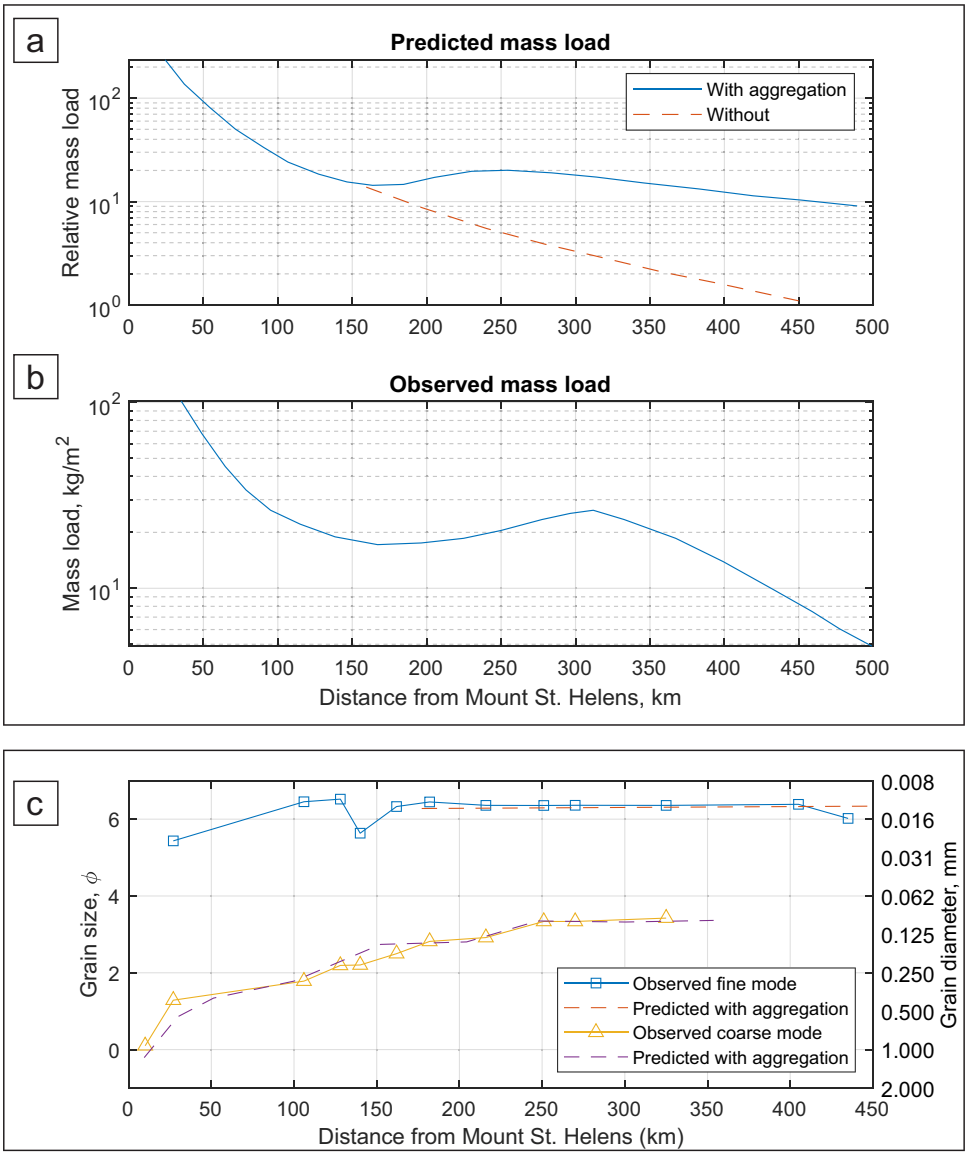

Fig. 9 (a) Predicted mass loading of the Mount St. Helens fall deposit using the tephra dispersal model of Carey and Sigurdsson (1982), with and without particle aggregation. (b) Observed mass loading of the Mount St. Helens fall deposit along the main dispersal axis from Sarna-Wojcicki et al. (1981). (c) Predicted (solid lines) and observed (dashed lines) values of the coarse and fine modes of the Mount St. Helens deposit along the main dispersal axis. After Carey and Sigurdsson (1982)

fine ash significantly reduces the atmospheric residence time of particulates and thus partially mitigates in-flight hazards to aircraft. Aggregation can result in localized higher deposition of fine ash, leading to health impacts from respiratory problems or fouling of water supplies and other potential infrastructure damage (Wilson et al. 2015).

Premature fallout of fine ash causes bimodality of distal ash-fall deposits due to a combination of deposition of individual particles, usually coarser than 63 microns, and aggregates consisting fine ash (Carey and Sigurdsson 1982; Rose and Durant 2009). This result was supported by early modeling (Fig. 9c). Studies of other widespread tephra-fall layers demonstrate similar grain-size bimodality of distal deposits (Sparks and Huang 1980) and led to the recognition that aggregation and other enhanced sedimentation processes are common in tephra deposition (Brazier et al. 1983; Brown et al. 2012).

The Mount St. Helens event set the standard for analyzing the total grain-size distribution of a large-magnitude explosive eruption and shed new light on how the fine-ash component constrains fragmentation processes. Based on an early granulometric application of the Coulter Counter Method (Graham 2003), Carey and Sigurdsson (1982) showed that more than 60% of the May 18 deposit consisted of fragments 63 microns or smaller. A later compilation (Rust and Cashman 2011) showed this to be among the most fine-enriched deposits yet sampled. It is now thought that the fine-ash component of the 1980 fall deposit was enhanced by the substantial addition of fragments milled during blast co-PDC activity (Eychenne et al. 2015), similar to other large, co-PDC deposits (e.g., Sparks and Huang 1980; Wilson 2001; Wiesner et al. 2004; Engwell et al. 2014; Engwell and Eychenne 2016).

Other insights

The 1980 eruptions of Mount St. Helens also spawned two new fields of study associated with ashfall: ash resuspension and impacts to human health and agriculture. While these topics are outside the scope of this article, they are too important to completely ignore. Airborne measurements of resuspended ash in the atmosphere after 18 May for example (Hobbs et al. 1983) were among the first ever made, showing that wind speeds of only a few meters per second could pick up recently deposited ash and reduce visibility. Air quality monitoring stations set up throughout Washington State in 1980 provided some of the first-ever measurements of total suspended particulates (TSP) during an ashfall event. The 8-h average TSP in Yakima on 18 May, 33.8 mg/m^3, remains the highest measured during any ashfall event anywhere (Bernstein et al. 1986). From 18 through 25 May, resuspension kept daily TSP values in Yakima above the U.S. Environmental Protection Agency's Emergency Action Level of 0.8 mg/m^3 (Bernstein et al. 1986). At Yakima's two major hospitals, visits per day to the Emergency Room due to asthma and/or bronchitis rose nearly an order of magnitude above normal on 19 May and remained above normal for more than two weeks. These observations motivated some of the first studies of effects of ash on human health (e.g., Baxter et al. 1981). Heavy ashfall over the agricultural college of Washington State University in Pullman prompted important first studies of the effects ash on agriculture (Cook et al. 1981; Johansen et al. 1981; Lyons 1986) and on range and forest land (Folsom 1986). Since 1980, resuspension events at other volcanoes such as Eyjafjallajökull (Leadbetter et al. 2012; Thorsteinsson et al. 2012; Liu et al. 2014), the Valley of Ten Thousand Smokes in Alaska (Hadley et al. 2004; Wallace and Schwaiger 2019), and Cordòn Caulle volcano, Chile (Folch et al. 2014; Mingari et al. 2020), demonstrate that ash-resuspension problems can be chronic and widespread. Similarly, areas of chronic ashfall such as at Montserrat (Searl et al. 2002; Horwell et al. 2003) or Merapi (Damby et al. 2013) have spawned extensive studies of volcanic ash health hazards (Horwell and Baxter 2006).

How Mount St. Helens changed our understanding of ash transport and deposition

The discussions below summarize how Mount St. Helens improved our understanding of volcanic processes and our ability to anticipate and forecast hazards but are by no means comprehensive. Some aspects of what we learned, for example, about effects of ash resuspension and post-event impacts to health, are covered in greater detail by Damby et al. (this volume).

Co-PDC clouds

Observations made during the Mount St. Helens eruption provided critical insights into the origin, and behavior, of buoyant clouds formed from ground-hugging PDCs. Before the Mount St. Helens eruption, evidence for co-PDC clouds came from the analyses of ancient ignimbrite and fall deposits, whose componentry (enrichment in crystals in ignimbrites), grain size, and stratigraphy (homogeneous fine ashfall deposits) suggested that, during emplacement of PDCs, significant elutriated clouds formed (e.g., Sparks and Walker, 1977). The giant umbrella cloud formed by the lift-off of the blast PDC during the Mount St. Helens eruption provided the first direct observation of these processes from a PDC (Sparks et al. 1986). It also demonstrated that elutriated co-PDC clouds reached similar (or even greater) heights than vent-derived columns, contributing significantly to the fallout volume and influencing grain size and componentry characteristics of fallout deposits (Eychenne et al. 2015). The early interpretations of the Mount St. Helens plume

dynamics (both the early blast co-PDC cloud and co-PDC plumes from later phases) informed the interpretation of other deposits, including from the Pinatubo eruption in 1991 (Holasek et al. 1996), and eruptions in the geological record that lack direct evidence for co-ignimbrite clouds (Engwell and Eychenne 2016).

Umbrella cloud growth

Umbrella growth relationships derived from the Mount St. Helens observations (Sparks et al. 1986) have been generalized and combined with theoretical relations for steady growth derived from Pinatubo (e.g., Sparks et al. 1997, ch. 11). The theory has been applied to estimate mass eruption rate of eruptions (Pouget et al. 2013; Van Eaton et al. 2016; Hargie et al. 2019), a key parameter used to model ash-cloud concentration for aviation safety (e.g., Beckett et al. 2020). The advection of ash in the upwind (Sparks et al. 1986) and crosswind directions (Bursik et al. 1992a) inferred in 1980 has been considered for much larger eruptions since the Pinatubo event (Koyaguchi and Tokuno 1993), with the recognition that eruptions of size VEI 6 or larger on the Volcanic Explosivity Index (Newhall and Self 1982) are likely to produce large, circular clouds and deposits that differ qualitatively from the oblong and fan-shaped features associated with weak plumes. Such giant umbrella clouds may be subject to Coriolis forces that increase areal dispersion and reduce the sensitivity of dispersion to prevailing wind directions or plume height (Baines and Sparks 2005; Mastin et al. 2014). For example, umbrella growth may account for Yellowstone tephra deposits that lie 2000 km upstream of prevailing winds (Mastin et al. 2014).

Ash aggregation

The correlation between a secondary thickness maximum and aggregation was first made at Mount St. Helens (Carey and Sigurdsson 1982). Observations of ash aggregates in the proximal and distal May 18 deposit have motivated laboratory and field-based studies of aggregation for several decades (Sorem 1982; Gilbert and Lane 1994; Schumacher 1994; Schumacher and Schmincke 1995; Veitch and Woods 2001; James et al. 2002, 2003; Textor et al. 2006a, 2006b; Durant et al. 2009; Rose and Durant 2011; Brown et al. 2012; Telling and Dufek 2012; Telling et al. 2013; Durant 2015; Bagheri et al. 2016; Durant and Brown 2016; Mueller et al. 2017; Pollastri et al. 2021). For example, Schumacher (1994) sought to reproduce the "Sorem clusters" that fell in eastern Washington using laboratory experiments of charged ash particles, and the secondary thickness maximum described by Carey and Sigurdsson (1982) is often cited to demonstrate how aggregation can impact the large-scale structure of fall deposits.

Influence on operational tephra forecasting

Throughout 1980 and beyond, multiple explosive eruptions of Mount St. Helens sent ash in many different directions (Sarna-Wojcicki et al. 1981). Portland, Oregon, located southwest of the volcano, was assumed to be mostly safe from ashfall in the pre-1980 hazard assessment (Crandell and Mullineaux 1978), but was affected on 12 June and 17 October. The 12 June event required removal of 5300 m^3 of ash from more than 2400 km of city streets (Schuster 1981). Many communities inundated by ash on 18 May and subsequent events were caught by surprise, as State emergency managers and the USGS were concentrating communication efforts on local counties where impacts were greater (Warrick et al. 1981).

The widespread impact of ash raised the importance of producing daily forecasts that could show areas at risk when an eruption occurred. Thus, from late March 1980 through to the end of 1981, the USGS ran an early and pioneering NOAA forecast model (Heffter et al. 1975) that would interpolate wind trajectories at different elevations (Fig. 10a) (Miller et al. 1981). These efforts heralded major modeling advances in the next few decades.

From the 1980s through the 1990s, models that calculate tephra sedimentation became common in volcanology (e.g., Carey and Sigurdsson 1982; Suzuki 1983; Hopkins and Bridgman 1985; Carey and Sparks 1986; Armienti et al. 1988; Glaze and Self 1991; Bursik et al. 1992b; Sparks et al. 1992; Hurst 1994; Bonadonna et al. 1998). Most such models solved for advection and diffusion semi-analytically (e.g., Hurst 1994) or, in weak plumes, by calculating air entrainment and particle settling (e.g., Bonadonna et al. 2005). Given a specified plume height, erupted volume, grain-size distribution, and one-dimensional wind sounding, they can produce theoretical isopach maps. Many of these models were validated by comparing with the Mount St. Helens deposit data (Carey and Sigurdsson 1982; Hopkins and Bridgman 1985; Armienti et al. 1988; Glaze and Self 1991; Bonadonna and Phillips 2003). During the next phase at Mount St. Helens from 2004 to 2008, the USGS employed the ashfall model (Hurst 1994) for daily forecasting (Fig. 10b).

In parallel efforts, from the 1980s into the 2000s, the meteorological community developed three-dimensional dispersal models to track the path of pollutant clouds (Draxler and Hess 1998; Jones 2004; Daniele et al. 2009; Folch et al. 2009; Stein et al. 2015). These models differ from the above-described models in that they use a three-dimensional time-varying wind field, are fully numerical, slower than one-dimensional semi-analytical models (running over minutes to hours versus seconds for the latter). These models can forecast cloud movement as well as ashfall and can simulate very large or long-lived eruptions in

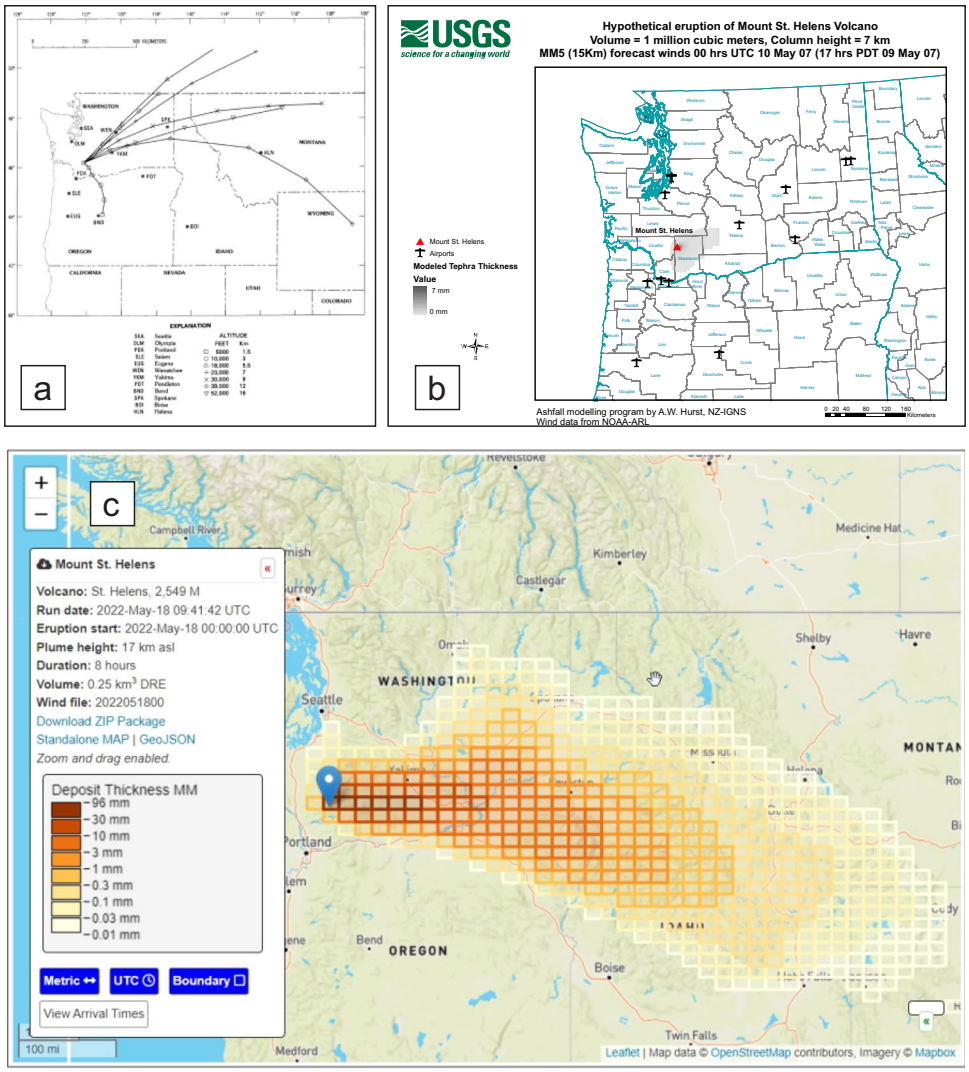

Fig. 10 Three generations of models used at the USGS Cascades Volcano Observatory. (a) Example wind trajectory forecast of the type generated daily in 1980 (from Miller et al. (1981)). This forecast uses the wind field available for 18 May 1980, 11:00 PDT. The first two symbols on each altitude track show positions of airborne ash 3 h apart; symbols farther along each track show positions at 6-h intervals. (b) Hypothetical eruption forecast using the semi-analytical ashfall model (Hurst 1994), assuming a tephra volume of 1 million cubic meters and plume height of 7 km. Forecasts of this type were produced daily during the 2004–2008 eruption of Mount St. Helens. (c) Modern model forecast of the hypothetical cloud from a 18 May-sized eruption, assuming the eruption occurred on 18 May 2022, at 0000 UTC. Plot is generated using the Ash3d model, which uses a fully three-dimensional, time-varying wind field (Schwaiger et al. (2012); https://vsc-ash.wr.usgs.gov/Ash3d). Results of this type are generated daily and posted online for instructional purposes (https://www.usgs.gov/volcanoes/mount-st.-helens/ash-cloud-simulations-what-if-mount-st-helens-produced-explosive). Similar results are automatically generated twice daily for all U.S. volcanoes in a state of unrest. Results of each simulation also include animations of cloud movement, maps of cloud height, arrival time, and tables of ash arrival time, ashfall thickness, and fall duration at regional airports

changing wind fields. Today, these models are the core tools used to forecast ash-cloud movement for aviation safety. Many of them consider key processes highlighted in the Mount St. Helens eruption such as particle aggregation (Costa et al. 2010; Folch et al. 2010; Beckett et al. 2022) and umbrella growth (Costa et al. 2013; Mastin et al. 2014; Webster et al. 2020).

The literature on plume dynamics, tephra transport, and deposition has grown hugely, and a complete up-to-date review is out of the scope here. Some publications that summarize developments over the four decades since 1980 include Sparks et al. (1997), Bonadonna et al. (2012), and Folch (2012).

Influence on ash and aviation hazards

Concern over ash and aviation safety can be traced back to Mount St. Helens. The 18 May 1980 eruption caused the

cancellation of nearly 1400 flights and damaged nine aircraft in flight—among the most of any historical eruption behind Eyjafjallajökull in 2010 (Guffanti et al. 2010; Christmann et al. 2017). The first recorded case of in-flight engine damage occurred on 25 May when an L-100 aircraft flew into a plume over the volcano (Gabbard et al. 1982; Guffanti et al. 2010).

In 1980, the NWS Forecast Office in Seattle forecast ash-cloud movement using interpolated NOAA-based wind trajectories, similar to the USGS forecasts (Miller et al., 1981). Nearly two decades later, as Volcanic Ash Advisory Centers (VAACs) were established (Servranckx et al. 1999), national meteorological agencies adapted their three-dimensional dispersion models to track the movement of volcanic ash clouds. Examples include the Met Office NAME model (Jones 2004), the NOAA Hysplit model (Stein et al. 2015), the Canadian CANERM model (now MLDP0, D'Amours et al. (2015)), and the Meteo France model MOCAGE Accident (Sič et al. 2015). In the late 2000s and early 2010s, two additional 3D models, Fall3d (Folch et al. 2009) and Ash3d (Schwaiger et al. 2012), were developed specifically for ash deposition and movement of volcanic clouds. They too were validated by comparison with the Mount St. Helens 1980 deposit data (Folch et al. 2010; Mastin et al. 2016).

Today, tephra dispersal models are used by both volcano observatories and VAACs. User interfaces (Bear-Crozier et al. 2012; Mastin et al. 2013; Palma et al. 2014) make them usable to all volcano observatory staff during unrest (Coombs et al. 2019) or as instructional tools (e.g., Fig. 10c). In 1980, it took about an hour for an operator to connect remotely to a NOAA server, run the model, and generate a map. Today, daily Ash3d simulations for all Alaska volcanoes at a state of unrest are generated and posted automatically (https://www.avo.alaska.edu/).

Discussion and remaining questions

Based on both plume height and volume, the 18 May 1980 eruption ranked 5 on the VEI scale. On average, VEI 5+ eruptions occur once or twice per decade (Deligne et al. 2010). The growth of umbrella clouds, climatic effects, societal impacts of tephra fallout and reworking, physics of shock waves and tsunamis are just a few examples of phenomena associated with such large eruptions. In addition, large eruptions attract widespread attention and observations that help science surge forward. Thus, the size of the Mount St. Helens eruption and the attention it garnered partially explain why we learned so much. But even among eruptions this size, its impact was large, and it seems appropriate to ask why.

Since 1980, there have been only four or five eruptions ranked VEI 5 or larger by the Smithsonian Institution's Global Volcanism Program (https://volcano.si.edu/): El Chichón (1982) (Sigurdsson et al. 1984), Hudson (1991) (Scasso et al. 1994), Pinatubo (1991) (Wiesner et al. 2004), Puyahue-Cordòn Caulle (2011) (Pistolesi et al. 2015), and Hunga-Tonga Hunga Ha'apai (HTHH, 2022) (Terry et al. 2022). Each eruption taught important lessons about the nature and consequences of large eruptions. Pinatubo for example demonstrated the power of large umbrella clouds in dispersing tephra (Koyaguchi and Tokuno 1993). HTHH provided the first modern data on global volcanogenic tsunamis (Carvajal et al. 2022) and atmospheric waves (Matoza et al. 2022). Sulfur dioxide emissions could be measured with increasing accuracy during each eruption and used to calibrate the cooling effect of SO_2 on climate (Carn et al. 2016). Yet none of these subsequent eruptions could be directly observed as well as Mount St. Helens in 1980. Hudson and HTHH were too remote. Puyahue Cordòn Caulle was also remote and is ranked VEI 5 only because its several VEI 3–4 events are aggregated into a single eruption (Pistolesi et al. 2015). Major phases of El Chichón occurred at night and destroyed nearby villages of observers (Sigurdsson et al. 1984). Pinatubo erupted during a major typhoon. Large eruptions are infrequent; and the well-observed ones are rarer still.

Many questions raised by the 1980 Mount St. Helens eruption remain. For example, what controlled the size and density of aggregates? How has the tephra-fall deposit degraded over time? How many of the tephra eruptions of 1980 could we identify in the stratigraphic record, using only exposures available today? These questions await further study.

Conclusions

The 18 May 1980 Mount St. Helens eruption taught us more about tephra transport and sedimentation than just about any other in the past half-century. The rich observations launched a new era of research on tephra transport and forecasting of tephra hazards. Many phenomena were highlighted, such as the growth of umbrella clouds, aggregation processes, and hydrometeor formation. These are now regarded as first-order processes essential to consider in forecasting and modeling tephra hazards. The pioneering use of dispersion models has evolved into a core component of tephra-hazard forecasting. The disruptive effects of ash on flight operations helped motivate the development of a global infrastructure to forecast ash-cloud movement for aviation safety. Every eruption teaches us something new. But the abundant observations and significant impacts of 18 May 1980 made it a singular teaching event.

Supplementary Information The online version contains supplementary material available at https://doi.org/10.1007/s00445-022-01613-0.

Acknowledgements We owe a particular debt to the few scientists who were involved in the 1980 response and were still available to share their recollections during preparation of this report. Among these are Carolyn Driedger, Michael Doukas, Richard Waitt, Thomas Murray, Ed Brown, and Tom Casadevall of the USGS. Spencer Wood (Boise State Univ., retired) drove the north-south transect just east of the Idaho-Washington border in 1980 and kindly sent us the photo of aggregates on the roadway in Fig. 5. Tom Murray and Ed Brown shared their experiences in preparing daily model forecasts in 1980 that are illustrated in Fig. 10a. Carolyn Driedger, Tom Casadevall, Mike Doukas, and Richard Waitt shared their experiences collecting tephra. We also thank reviewers Kristi Wallace Costanza Bonadonna, and Britta Jensen.

Declarations

Disclaimer Any use of trade, firm, or product names is for descriptive purposes only and does not imply endorsement by the U.S. Government.

References

Armienti P, Macedonio G, Pareschi MT (1988) A numerical model for simulation of tephra transport and deposition: applications to May 18, 1980, Mount St. Helens eruption. J Geophys Res 93(B6):6463–6476. https://doi.org/10.1029/JB093iB06p06463

Aubry TJ, Engwell S, Bonadonna C, Carazzo G, Scollo S, Van Eaton AR, Taylor IA, Jessop D, Eychenne J, Gouhier M, Mastin LG, Wallace KL, Biass S, Bursik M, Grainger RG, Jellinek AM, Schmidt A (2021) The Independent Volcanic Eruption Source Parameter Archive (IVESPA, version 1.0): A new observational database to support explosive eruptive column model validation and development. J Volcanol Geotherm Res 417:107295. https://doi.org/10.1016/j.jvolgeores.2021.107295

Bagheri G, Rossi E, Biass S, Bonadonna C (2016) Timing and nature of volcanic particle clusters based on field and numerical investigations. J Volcanol Geotherm Res 327:520–530. http://www.sciencedirect.com/science/article/pii/S0377027316303547

Baines PG, Sparks RSJ (2005) Dynamics of giant volcanic ash clouds from supervolcanic eruptions. Geophys Res Lett 32(24):L24808

Baxter PJ, Ing R, Falk H, French J, Stein GF, Bernstein RS, Merchant JA, Allard J (1981) Mount St Helens eruptions, May 18 to June 12, 1980: an overview of the acute health impact. JAMA 246(22):2585–2589. https://doi.org/10.1001/jama.1981.03320220035021

Baxter PJ, Ing R, Falk H, Plikaytis B (1983) Mount St. Helens eruptions: the acute respiratory effects of volcanic ash in a North American community. Arch Environ Health: An Int J 38(3):138–143. https://doi.org/10.1080/00039896.1983.10543994

Bear-Crozier A, Kartadinata N, Heriwaseso A, Nielson O (2012) Development of python-FALL3D: a modified procedure for modelling volcanic ash dispersal in the Asia-Pacific region. Nat Hazards 64(1):828–838. https://doi.org/10.1007/s11069-012-0273-7

Beckett F, Rossi E, Devenish B, Witham C, Bonadonna C (2022) Modelling the size distribution of aggregated volcanic ash and implications for operational atmospheric dispersion modelling. Atmos Chem Phys 22(5):3409–3431. https://doi.org/10.5194/acp-22-3409-2022

Beckett FM, Witham CS, Leadbetter SJ, Crocker R, Webster HN, Hort MC, Jones AR, Devenish BJ, Thomson DJ (2020) Atmospheric dispersion modelling at the London VAAC: a review of developments since the 2010 Eyjafjallajökull volcano ash cloud. Atmosphere 11(4):352. https://doi.org/10.3390/atmos11040352

Bernstein RS, Baxter PJ, Falk H, Ing R, Foster L, Frost F (1986) Immediate public health concerns and actions in volcanic eruptions: lessons from the Mount St. Helens eruptions, May 18-October 18, 1980. Am J Public Health 76(Suppl):25–37. https://doi.org/10.2105/AJPH.76.Suppl.25

Blackburn EA, Wilson L, Sparks RSJ (1976) Mechanisms and dynamics of strombolian activity. J Geol Soc 132(4):429–440. https://doi.org/10.1144/gsjgs.132.4.0429

Blundy J, Cashman KV (2001) Ascent-driven crystallization of dacite magmas at Mount St. Helens, 1980–86. Contrib Miner Petrol 140:631–650. https://doi.org/10.1007/s004100000219

Bonadonna C, Ernst GGJ, Sparks RSJ (1998) Thickness variations and volume estimates of tephra fall deposits: the importance of particle Reynolds number. J Volcanol Geoth Res 81:173–187. https://doi.org/10.1016/S0377-0273(98)00007-9

Bonadonna C, Folch A, Loughlin S, Puempel H (2012) Future developments in modelling and monitoring of volcanic ash clouds: outcomes from the first IAVCEI-WMO workshop on Ash Dispersal Forecast and Civil Aviation. Bull Volcanol 74:1–10. https://doi.org/10.1007/s00445-011-0508-6

Bonadonna C, Phillips JC (2003) Sedimentation from strong volcanic plumes. Journal of Geophysical Research: Solid Earth 108(B7):2340. https://doi.org/10.1029/2002JB002034

Bonadonna C, Phillips JC, Houghton BF (2005) Modeling tephra sedimentation from a Ruapehu weak plume eruption. J Geophys Res 110(B08209): https://doi.org/10.1029/2004JB003515. https://doi.org/10.1029/2004JB003515

Brazier S, Sparks RSJ, Carey SN, Sigurdsson H, Westgate JA (1983) Bimodal grain size distribution and secondary thickening in air-fall ash layers. Nature 301:115–119

Brown RJ, Bonadonna C, Durant AJ (2012) A review of volcanic ash aggregation. Phys Chem Earth, Parts A/B/C 45–46(0):65–78. http://www.sciencedirect.com/science/article/pii/S1474706511003172

Brown RJ, Branney MJ, Maher C, Davila-Harris P (2009) Origin of accretionary lapilli within ground-hugging density currents: evidence from pyroclastic couplets on Tenerife. Geol Soc Am Bull 122(1–2):305–320

Bursik MI, Carey SN, Sparks RSJ (1992a) A gravity current model for the May 18, 1980 Mount St. Helens plume. Geophys Res Lett 19(16):1663–1666. http://www.agu.org/journals/gl/v019/i016/92GL01639/

Bursik MI, Sparks RSJ, Gilbert JS, Carey SN (1992b) Sedimentation of tephra by volcanic plumes: I. Theory and its comparison with a study of the Fogo A plinian deposit, Sao Miguel (Azores). Bull Volcanol 54:329–344. https://doi.org/10.1007/BF00301486

Calder ES, Sparks RSJ, Woods AW (1997) Dynamics of co-ignimbrite plumes generated from pyroclastic flows of Mount St. Helens (7 August 1980). Bull Volcanol 58(6):432–440. https://doi.org/10.1007/s004450050151

Carey S, Sigurdsson H (1982) Influence of particle aggregation on deposition of distal tephra from the May 18, 1980, eruption of Mount St. Helens volcano. J Geophys Res 87(B8):7061–7072. https://doi.org/10.1186/s40623-020-01233-y

Carey S, Sigurdsson H, Gardner JE, Criswell W (1990) Variations in column height and magma discharge during the May 18, 1980 eruption of Mount St. Helens. J Volcanol Geoth Res 43:99–112. https://doi.org/10.1016/0377-0273(90)90047-J

Carey S, Sparks RSJ (1986) Quantitative models of the fallout and dispersal of tephra from volcanic eruption columns. Bull Volcanol 48:109–125. https://doi.org/10.1007/BF01046546

Carn SA, Clarisse L, Prata AJ (2016) Multi-decadal satellite measurements of global volcanic degassing. J Volcanol Geoth Res 311:99–134. https://doi.org/10.1016/j.jvolgeores.2016.01.002

Carvajal M, Sepúlveda I, Gubler A, Garreaud R (2022) Worldwide signature of the 2022 Tonga volcanic tsunami. Geophys Res Lett 49(6):e2022GL098153. https://agupubs.onlinelibrary.wiley.com/doi/abs/10.1029/2022GL098153

Christiansen RL, Peterson DW (1981) Chronology of the eruptive activity. In: Lipman PW, Mullineaux DR (eds) The 1980 eruptions of Mount St. Helens, Washington: USGS professional paper 1250. U.S. Government Printing Office, Washington, D.C., pp 3–30, https://doi.org/10.3133/pp1250

Christmann C, Nunes RR, Schmitt AR, Guffanti M (2017) Flying into volcanic ash clouds: an evaluation of hazard potential. In, STO-MP-AVT-272: Impact of Volcanic Ash Clouds on Military Operations, Vilnius. https://www.sto.nato.int/publications/STO%20Meeting%20Proceedings/Forms/Meeting%20Proceedings%20Document%20Set/docsethomepage.aspx?ID=42946&FolderCTID=0x0120D5200078F9E87043356C409A0D30823AFA16F602008CF184CAB7588E468F5E9FA364E05BA5&List=7e2cc123-6186-4c30-8082-1ba072228ca7&RootFolder=/publications/STO%20Meeting%20Proceedings/STO-MP-AVT-272

Cook RJ, Barron JC, Papendick RI, Williams GJ (1981) Impact on agriculture of the Mount St. Helens eruptions. Science 211(4477):16–22. https://www.jstor.org/stable/1685507

Coombs M, Wallace K, Cameron C, Lyons J, Wech A, Angeli K, Cervelli P (2019) Overview, chronology, and impacts of the 2016–2017 eruption of Bogoslof volcano, Alaska. Bull Volcanol 81(11):62. https://doi.org/10.1007/s00445-019-1322-9

Costa A, Folch A, Macedonio G (2010) A model for wet aggregation of ash particles in volcanic plumes and clouds: 1. Theoretical formulation. J Geophys Res 115:B09201. https://doi.org/10.1029/2009JB007175

Costa A, Folch A, Macedonio G (2013) Density-driven transport in the umbrella region of volcanic clouds: implications for tephra dispersion models. Geophys Res Lett 40(18):4823–4827. https://doi.org/10.1002/grl.50942

Crandell D, Mullineaux DR (1978) Potential hazards from future eruptions of Mount St. Helens volcano, Washington. U.S. Geological Survey Bulletin 1383-C. U.S. Government Printing Office, Washington, D.C., p 26, https://doi.org/10.3133/b1383C

Crandell D, Mullineaux DR, Miller RD, Rubin M (1962) Pyroclastic deposits of Recent age at Mount Rainier, Washington. U.S. Geological Survey Professional Paper 450-D. U.S. Government Printing Office, Washington D.C., pp D64–68,

Crandell DR (1963) Paradise debris flow at Mount Rainier, Washington. pp B135-B139,

Crandell DR, Waldron HH (1956) A recent volcanic mudflow of exceptional dimensions from Mount Rainier, Washington. Am J Sci 254(6):349–362. https://doi.org/10.2475/ajs.254.6.349

Criswell W (1987) Chronology and pyroclastic stratigraphy of the May 18, 1980 eruption of Mount St. Helens, Washington. J Geophys Res 92(B10):10237–10266. https://doi.org/10.1029/JB092iB10p10237

Cutler NA, Streeter RT, Dugmore AJ, Sear ER (2021) How do the grain size characteristics of a tephra deposit change over time? Bull Volcanol 83(7). https://doi.org/10.1007/s00445-021-01469-w

Cutler NA, Streeter RT, Engwell SL, Bolton MS, Jensen BJL, Dugmore AJ (2020) How does tephra deposit thickness change over time? A calibration exercise based on the 1980 Mount St Helens tephra deposit. J Volcanol Geotherm Res 399:106883. https://www.sciencedirect.com/science/article/pii/S0377027319305773

Cutler NA, Streeter RT, Marple J, Shotter LR, Yeoh JS, Dugmore AJ (2018) Tephra transformations: variable preservation of tephra layers from two well-studied eruptions. Bull Volcanol 80(11):77. https://doi.org/10.1007/s00445-018-1251-z

D'Amours R, Malo A, Flesch T, Wilson J, Gauthier J-P, Servranckx R (2015) The Canadian Meteorological Centre's atmospheric transport and dispersion modelling suite. Atmos Ocean 49(1):1–24. https://doi.org/10.1080/07055900.2014.1000260

Damby DE, Horwell CJ, Baxter PJ, Delmelle P, Donaldson K, Dunster C, Fubini B, Murphy FA, Nattrass C, Sweeney S, Tetley TD, Tomatis M (2013) The respiratory health hazard of tephra from the 2010 Centennial eruption of Merapi with implications for occupational mining of deposits. Journal of Volcanology and Geothermal Research 261:376–387. http://www.sciencedirect.com/science/article/pii/S0377027312002673

Daniele P, Lirer L, Petrosino P, Spinelli N, Peterson R (2009) Applications of the PUFF model to forecasts of volcanic clouds dispersal from Etna and Vesuvio. Comput Geosci 35(5):1035–1049. https://doi.org/10.1016/j.cageo.2008.06.002

Danielsen EF (1981) Trajectories of the Mount St. Helens Eruption Plume Science 211(4484):819–821. https://doi.org/10.1126/science.211.4484.819

Day TG, Fisher JE (1980) Mt. St. Helens: how a wastewater plant coped with its aftermath. Journal (Water Pollution Control Federation) 52(8):2082–2089. http://www.jstor.org/stable/25040848

Degruyter W, Bonadonna C (2012) Improving on mass flow rate estimates of volcanic eruptions. Geophys Res Lett 39(16):L16308. https://doi.org/10.1029/2012GL052566

Deligne NI, Coles SG, Sparks RSJ (2010) Recurrence rates of large explosive volcanic eruptions. J Geophys Res: Solid Earth 115(B6). https://doi.org/10.1029/2009JB006554

Draxler RR, Hess GD (1998) An overview of the Hysplit-4 modeling system for trajectories, dispersion, and deposition. Aust Meteorol Mag 47(4):295–308. https://www.arl.noaa.gov/documents/reports/MetMag.pdf

Durant AJ (2015) RESEARCH FOCUS: toward a realistic formulation of fine-ash lifetime in volcanic clouds. Geology 43(3):271–272. https://doi.org/10.1130/focus032015.1

Durant AJ, Brown RJ (2016) Chapter 3 - ash aggregation in volcanic clouds. In: Mackie S, Cashman K, Ricketts H, Rust A, Watson M (eds) Volcanic Ash. Elsevier, pp 53–65, https://doi.org/10.1016/B978-0-08-100405-0.00006-9

Durant AJ, Rose WI, Sarna-Wojcicki AM, Carey S, Volentik AC (2009) Hydrometeor-enhanced tephra sedimentation: constraints from the 18 May 1980 eruption of Mount St. Helens (USA). J Geophys Res 114(B03204): https://doi.org/10.1029/2008JB005756

Engwell S, Eychenne J (2016) Chapter 4 - contribution of fine ash to the atmosphere from plumes associated with pyroclastic density currents. In: Mackie S, Cashman K, Ricketts H, Rust A, Watson M (eds) Volcanic Ash. Elsevier, pp 67–85, https://doi.org/10.1016/B978-0-08-100405-0.00007-0

Engwell SL, Sparks RSJ, Carey S (2014) Physical characteristics of tephra layers in the deep sea realm: the Campanian Ignimbrite eruption. Geol Soc London Spec Publ 398(1):47–64. https://doi.org/10.1144/sp398.7

Eychenne J, Cashman K, Rust A, Durant A (2015) Impact of the lateral blast on the spatial pattern and grain size characteristics of the 18 May 1980 Mount St. Helens fallout deposit. J Geophys Res: Solid Earth 120(9):6018–6038. https://doi.org/10.1002/2015JB012116

Fero J, Carey SN, Merrill JT (2008) Simulation of the 1980 eruption of Mount St. Helens using the ash-tracking model PUFF. J Volcanol Geotherm Res 175(3):355–366. https://doi.org/10.1016/j.jvolgeores.2008.03.029

Fisher RV, Schmincke H-U (1984) Pyroclastic rocks. Springer-Verlag, Berlin, p 472

Folch A (2012) A review of tephra transport and dispersal models: Evolution, current status, and future perspectives. J Volcanol Geoth Res 235–236:96–115. https://doi.org/10.1016/j.jvolgeores.2012.05.020

Folch A, Costa A, Durant A, Macedonio G (2010) A model for wet aggregation of ash particles in volcanic plumes and clouds: 2 Model Application. J Geophys Res 115(B9):B09202. https://doi.org/10.1029/2009JB007176

Folch A, Costa A, Macedonio G (2009) FALL3D: A computational model for transport and deposition of volcanic ash. Comput Geosci 35(6):1334–1342. https://doi.org/10.1016/j.cageo.2008.08.008

Folch A, Mingari L, Osores MS, Collini E (2014) Modeling volcanic ash resuspension – application to the 14–18 October 2011 outbreak episode in central Patagonia, Argentina. Nat Hazards Earth Syst Sci 14(1):119–133. https://doi.org/10.5194/nhess-14-119-2014

Folsom MM (1986) Mount St. Helens tephra on range and forest lands of eastern Washington: local erosion and redeposition. In: Keller SAC (ed) Mount St. Helens: Five Years Later. Eastern Washington University Press, Spokane, pp 116–120,

Folsom MM, Quinn RR (1980) Ash from the May 18, 1980 eruption of Mount St. Helens: Washington Division of Geology and Earth Resources Open-File Report 80–12. https://www.dnr.wa.gov/programs-and-services/geology/publications-and-data/washington-geologic-survey-publications-catalog

Foo ZH, Jensen BJL, Bolton MSM (2020) Glass geochemical compositions from widespread tephras erupted over the last 200 years from Mount St. Helens. J Quat Sci 35(1–2):102–113. https://doi.org/10.1002/jqs.3166

Foxworthy BL, Hill M (1982) Volcanic eruptions of 1980 at Mount St. Helens: the first 100 days. USGS Prof. Paper 1249. U.S. Government Printing Office, Washington, D.C., https://doi.org/10.3133/pp1249

Gabbard CB, LeLevier RE, Parry JFW (1982) Dust-cloud effects on aircraft engines--emerging issues and new damage mechanisms. Technical Report DNA-TR-82–18. Defense Nuclear Agency, Washington, D.C., p 132, https://www.semanticscholar.org/paper/Dust-Cloud-Effects-on-Aircraft-Engines--Emerging-A-Gabbard-LeLevier/636e911bde9415f3b070bacadc61b290bacfc76b

Gardner JE, Andrews BJ, Dennen R (2017) Liftoff of the 18 May 1980 surge of Mount St. Helens (USA) and the deposits left behind. Bull Volcanol 79(1). https://doi.org/10.1007/s00445-016-1095-3

Gilbert JS, Lane SJ (1994) The origin of accretionary lapilli. Bull Volcanol 56:398–411. https://doi.org/10.1007/BF00326465

Glaze LS, Self S (1991) Ashfall dispersal for the 16 September 1986, eruption of Lascar, Chile, calculated by a turbulent diffusion model. Geophys Res Lett 18(7):1237–1240. https://doi.org/10.1029/91GL01501

Graham MD (2003) The Coulter principle: foundation of an industry. JALA: J Assoc Lab Autom 8(6):72–81. https://doi.org/10.1016/s1535-5535-03-00023-6

Guffanti M, Casadevall TJ, Budding K (2010) Encounters of aircraft with volcanic ash clouds: a compilation of known incidents, 1953–2009. U.S. Geological Survey Data Series 545. U.S. Government Printing Office, Washington, D.C., p 16, http://pubs.usgs.gov/ds/545/

Hadley D, Hufford GL, Simpson JJ (2004) Resuspension of relic volcanic ash and dust from Katmai: still an aviation hazard. Weather and Forecasting 19(5):829–840. http://journals.ametsoc.org/doi/abs/https://doi.org/10.1175/1520-0434%282004%29019%3C0829%3ARORVAA%3E2.0.CO%3B2

Hargie KA, Van Eaton AR, Mastin LG, Holzworth RH, Ewert JW, Pavolonis M (2019) Globally detected volcanic lightning and umbrella dynamics during the 2014 eruption of Kelud, Indonesia. J Volcanol Geoth Res 382:81–91. https://doi.org/10.1016/j.jvolgeores.2018.10.016

Harris DM, Rose WI, Roe R, Thompson MR (1981) Radar observations of ash eruptions. In: Lipman PW, Mullineaux DR (eds) The 1980 Eruptions of Mount St. Helens, Washington: USGS Professional Paper 1250. U.S. Government Printing Office, Washington, D.C., pp 323–333, https://doi.org/10.3133/pp1250

Heffter JL, Taylor AD, Ferber GJ (1975) A regional-continental scale transport, diffusion, and deposition model. NOAA Air Resources Laboratories Tech. Memo. ERL ARL-50. National Oceanic and Atmospheric Administration, College Park, MD, p 28, https://www.arl.noaa.gov/documents/reports/ARL-50.PDF

Hildreth W, Drake RE (1992) Volcán Quizapu, Chilean Andes. Bull Volcanol 54:93–125. https://doi.org/10.1007/BF00278002

Hobbs PV, Hegg DA, Radke LF (1983) Resuspension of volcanic ash from Mount St. Helens. J Geophys Res: Oceans 88(C6):3919–3921. https://doi.org/10.1029/JC088iC06p03919

Hoblitt RP (2000) Was the 18 May 1980 lateral blast at Mt St. Helens the product of two explosions? Philos Trans R Soc Lond 358:1639–1661. https://doi.org/10.1098/rsta.2000.0608

Holasek RE, Self S (1995) GOES weather satellite observations and measurements of the May 18, 1980, Mount St. Helens eruption. J Geophys Res 100(B5):8469–8487. https://doi.org/10.1029/94JB03137

Holasek RE, Self S, Woods AW (1996) Satellite observations and interpretation of the 1991 Mount Pinatubo eruption plumes. J Geophys Res 101(B12):27635–27656. https://doi.org/10.1029/96JB01179

Hopkins A, Bridgman C (1985) A volcanic ash transport model and analysis of Mount St. Helens ashfall. J Geophys Res 90:10620–10630. https://doi.org/10.1029/JD090iD06p10620

Horwell CJ, Baxter PJ (2006) The respiratory health hazards of volcanic ash: a review for volcanic risk mitigation. Bull Volcanol 69(1):1–24. https://doi.org/10.1007/s00445-006-0052-y

Horwell CJ, Sparks RSJ, Brewer TS, Llewellin EW, Williamson BJ (2003) Characterization of respirable volcanic ash from the Soufrière Hills volcano, Montserrat, with implications for human health hazards. Bull Volcanol 65(5):346–362. https://doi.org/10.1007/s00445-002-0266-6

Hurst AW (1994) ASHFALL--A computer program for estimating volcanic ash fallout: report and users guide. Institute of Geological & Nuclear Sciences Report 94/23. p 14, https://citeseerx.ist.psu.edu/viewdoc/download?doi=10.1.1.527.1861&rep=rep1&type=pdf

James MR, Gilbert JS, Lane SJ (2002) Experimental investigation of volcanic particle aggregation in the absence of a liquid phase. J Geophys sRes: Solid Earth 107(B9):ECV 4–1-ECV 4–13. https://doi.org/10.1029/2001JB000950

James MR, Lane SJ, Gilbert JS (2003) Density, construction, and drag coefficient of electrostatic volcanic ash aggregates. J Geophys Res 108(B9):2435. https://doi.org/10.1029/2002JB002011

Jensen BJL, Beaudoin AB, Clynne MA, Harvey J, Vallance JW (2019a) A re-examination of the three most prominent Holocene tephra deposits in western Canada: Bridge River, Mount St. Helens Yn and Mazama. Quaternary International. https://doi.org/10.1016/j.quaint.2019.03.017

Jensen BJL, Polard-Yopek N, McGee T, Bolton MSM (2019b) Memories of ash: the May 18th 1980 Mount St. Helens eruption north of the border [abstr]. In, 2019b Fall American Geophysical Union Abstracts V23I-0301, https://agu.confex.com/agu/fm19/meetingapp.cgi/Paper/589102

Johansen CA, Eves JD, Mayer DF, Bach JC, Nedrow ME, Kious CW (1981) Effects of ash from Mt. St. Helens on bees. Melandria 37:20–29. http://pascal-francis.inist.fr/vibad/index.php?action=getRecordDetail&idt=PASCALZOOLINEINRA82X0100415

Jones A (2004) Atmospheric dispersion modelling at the Met Office. Weather 59(11):311–316. https://doi.org/10.1256/wea.106.04

Koyaguchi T, Tokuno M (1993) Origin of the giant eruption cloud of Pinatubo, June 15, 1991. J Volcanol Geoth Res 55:85–96. https://doi.org/10.1016/0377-0273(93)90091-5

Kuntz MA, Rowley PD, Macleod NS, Reynolds RL, McBroome LA, Kaplan AM, Lidke DJ (1981) Petrography and particle-size distribution of pyroclastic-flow, ash-cloud, and surge deposits. The 1980 eruptions of Mount St. Helens, Washington, U.S. Geological Survey professional paper 1250. U.S. Government Printing Office, Washington D.C., pp 525–540, https://doi.org/10.3133/pp1250

Larsen PO, von Ins M (2010) The rate of growth in scientific publication and the decline in coverage provided by Science Citation Index. Scientometrics 84(3):575–603. https://doi.org/10.1016/0377-0273(79)90051-9

Leadbetter SJ, Hort MC, von Löwis S, Weber K, Witham CS (2012) Modeling the resuspension of ash deposited during the eruption of Eyjafjallajökull in spring 2010. J Geophys Res: Atmospheres 117(D20):D00U10. https://doi.org/10.1029/2011JD016802

Liu EJ, Cashman KV, Beckett FM, Witham CS, Leadbetter SJ, Hort MC, Guðmundsson S (2014) Ash mists and brown snow: remobilization of volcanic ash from recent Icelandic eruptions. J Geophys Res: Atmospheres 119(15):9463–9480. https://doi.org/10.1002/2014JD021598

Lyons JV (1986) Agricultural impact and adjustment to Mount St. Helens ashfall: search for analogs. In: Keller SAC (ed) Mount St. Helens: Five Years Later. Eastern Washington University Press, Cheney, Washington, pp 423–429,

Mastin LG, Guffanti M, Servranckx R, Webley P, Barsotti S, Dean K, Durant A, Ewert JW, Neri A, Rose WI, Schneider D, Siebert L, Stunder B, Swanson G, Tupper A, Volentik A, Waythomas CF (2009) A multidisciplinary effort to assign realistic source parameters to models of volcanic ash-cloud transport and dispersion during eruptions. J Volcanol Geoth Res 186(1–2):10–21. https://doi.org/10.1016/j.jvolgeores.2009.01.008

Mastin LG, Randall M, J., Schwaiger H, Denlinger R (2013) User's guide and reference to Ash3d: a three-dimensional model for atmospheric tephra transport and deposition. U.S. Geological Survey Open-File Report 2013–1122. p 48, https://doi.org/10.3133/ofr20131122

Mastin LG, Van Eaton AR, Durant AJ (2016) Adjusting particle-size distributions to account for aggregation in tephra-deposit model forecasts. Atmos Chem Phys 16(14):9399–9420. https://doi.org/10.5194/acp-16-9399-2016

Mastin LG, Van Eaton AR, Lowenstern JB (2014) Modeling ash fall distribution from a Yellowstone supereruption. Geochem Geophys Geosyst 15(8):3459–3475. https://doi.org/10.1002/2014GC005469

Matoza RS, Fee D, Assink JD, Iezzi AM, Green DN, Kim K, Toney L, Lecocq T, Krishnamoorthy S, Lalande J-M, Nishida K, Gee KL, Haney MM, Ortiz HD, Brissaud Q, Martire L, Rolland L, Vergados P, Nippress A, Park J, Shani-Kadmiel S, Witsil A, Arrowsmith S, Caudron C, Watada S, Perttu AB, Taisne B, Mialle P, Le Pichon A, Vergoz J, Hupe P, Blom PS, Waxler R, De Angelis S, Snively JB, Ringler AT, Anthony RE, Jolly AD, Kilgour G, Averbuch G, Ripepe M, Ichihara M, Arciniega-Ceballos A, Astafyeva E, Ceranna L, Cevuard S, Che I-Y, De Negri R, Ebeling CW, Evers LG, Franco-Marin LE, Gabrielson TB, Hafner K, Harrison RG, Komjathy A, Lacanna G, Lyons J, Macpherson KA, Marchetti E, McKee KF, Mellors RJ, Mendo-Pérez G, Mikesell TD, Munaibari E, Oyola-Merced M, Park I, Pilger C, Ramos C, Ruiz MC, Sabatini R, Schwaiger HF, Tailpied D, Talmadge C, Vidot J, Webster J, Wilson DC (2022) Atmospheric waves and global seismoacoustic observations of the January 2022 Hunga eruption, Tonga. Science 377(6601):95–100. https://www.science.org/doi/abs/10.1126/science.abo7063

Menzel WP (2020) Chapter 2 - history of geostationary weather satellites. In: Goodman SJ, Schmit TJ, Daniels J, Redmon RJ (eds) The GOES-R Series. Elsevier, pp 5–11, https://doi.org/10.1016/B978-0-12-814327-8.00002-0

Miller CD, Mullineaux DR, Crandell DR (1981) Hazards assessments at Mount St. Helens. In: Lipman PW, Mullineaux DR (eds) The 1980 Eruptions of Mount St. Helens, Washington. USGS Professional Paper 1250. U.S. Government Printing Office, Washington, D.C., pp 789–802, https://doi.org/10.3133/pp1250

Mingari L, Folch A, Dominguez L, Bonadonna C (2020) Volcanic ash resuspension in Patagonia: numerical simulations and observations. Atmosphere 11(9):977. https://www.mdpi.com/2073-4433/11/9/977

Moore JG, Albee WC (1981) Topographic and structural changes, March-July 1980--Photogrammetric data. In: Lipman PW, Christiansen RL (eds) The 1980 Eruptions of Mount St. Helens, Washington. USGS Professional Paper 1250. U.S. Government Printing Office, Washington, D.C., pp 143–155, https://doi.org/10.3133/pp1250

Moore JG, Rice CJ (1984) Chronology and character of the May 18, 1980, explosive eruptions of Mount St. Helens. In: Explosive Volcanism: Inception, evolution and hazards. National Academy Press, Washington, D.C., pp 133–142,

Mueller SB, Kueppers U, Ametsbichler J, Cimarelli C, Merrison JP, Poret M, Wadsworth FB, Dingwell DB (2017) Stability of volcanic ash aggregates and break-up processes. Sci Rep 7(1):7440. https://doi.org/10.1038/s41598-017-07927-w

Newhall CG, Self S (1982 The volcanic explosivity index/VEI/- an estimate of explosive magnitude for historical volcanism .J Geophys Res 87https://doi.org/10.1029/JC087iC02p01231

Palma JL, Courtland L, Charbonnier S, Tortini R, Valentine GA (2014) Vhub: a knowledge management system to facilitate online collaborative volcano modeling and research. J Appl Volcanol 3(1):2. https://doi.org/10.1186/2191-5040-3-2

Pierson TC (1985) Initiation and flow behavior of the 1980 Pine Creek and Muddy River lahars, Mount St. Helens, Washington. Bull Geol Soc Am 96.

Pistolesi M, Cioni R, Bonadonna C, Elissondo M, Baumann V, Bertagnini A, Chiari L, Gonzales R, Rosi M, Francalanci L (2015) Complex dynamics of small-moderate volcanic events: the example of the 2011 rhyolitic Cordón Caulle eruption. Chile Bull Volcanol 77(1):1–24. https://doi.org/10.1007/s00445-014-0898-3

Pollastri S, Rossi E, Bonadonna C, Merrison JP (2021) Modelling the effect of electrification on volcanic ash aggregation. Frontiers in Earth Science 8(574106). https://www.frontiersin.org/articles/https://doi.org/10.3389/feart.2020.574106/full

Pouget S, Bursik M, Webley P, Dehn J, Pavolonis M (2013) Estimation of eruption source parameters from umbrella cloud or downwind plume growth rate. J Volcanol Geoth Res 258:100–112. https://doi.org/10.1016/j.jvolgeores.2013.04.002

Prata AJ (1989) Infrared radiative transfer calculations for volcanic ash clouds. Geophys Res Lett 16(11):1293–1296. https://doi.org/10.1029/GL016i011p01293

Rice CJ (1981) Satellite observations of the Mt. St. Helens eruption of 18 May 1980. Technical Report, Aerosp. Corp., Space Sci. Lab., El Segundo, CA,

Rose WI, Durant A (2009) Fine ash content of explosive eruptions. J Volcanol Geoth Res 186(1–2):32–39. https://doi.org/10.1016/j.jvolgeores.2009.01.010

Rose WI, Durant AJ (2011) Fate of volcanic ash: aggregation and fallout. Geology 39(9):895–896. http://geology.gsapubs.org

Rosenbaum J, Waitt R (1981) A summary of eyewitness accounts of the May 18 eruption. In: Lipman PW, Mullineaux DR (eds) The 1980 eruptions of Mount St. Helens, Washington. USGS Professional Paper 1250. U.S. Government Printing Office, Washington, D.C., pp 53–67, https://doi.org/10.3133/pp1250

Rosenfeld CL (1980) Observations on the Mount St. Helens eruption. American Scientist 68(September-October, 1980):494–509. https://doi.org/10.2307/27850039

Rust AC, Cashman KV (2011) Permeability controls on expansion and size distributions of pyroclasts. Journal of Geophysical Research: Solid Earth 116(11). https://doi.org/10.1029/2011JB008494

Rutherford MJ, Sigurdsson H, Carey S, Davis A (1985) The May 18, 1980, eruption of Mount St. Helens: 1, melt composition and experimental phase equilibria. Journal of Geophysical Research 90(B4):2929–2947. https://doi.org/10.1029/JB090iB04p02929

Sarna-Wojcicki AM, Shipley S, Waitt R, Dzurisin D, Hays WH, Davis JO, Wood SH, Bateridge T (1980) Areal distribution, thickness, and volume of downwind ash from the May 18, 1980 eruption of Mount St. Helens. U.S. Geological Survey Open-file Report 80–1078. U.S. Government Printing Office, Washington, D.C., p 15, file://C%3A%2Fjournal%20pdf%27s%2FCascades%2FSt.%20Helens%2F1980%2FSarna-Wojcicki%20et%20al.,%201981.pdf

Sarna-Wojcicki AM, Shipley S, Waitt R, Dzurisin D, Wood SH (1981) Areal distribution, thickness, mass, volume, and grain size of air-fall ash from the six major eruptions of 1980. In: Lipman PW, Christiansen RL (eds) The 1980 Eruptions of Mount St. Helens, Washington; U.S. Geological Survey Professional Paper 1250. U.S. Government Printing Office, Washington, D.C., pp 577–601, https://doi.org/10.3133/pp1250

Scasso RA, Corbella H, Tiberi P (1994) Sedimentological analysis of the tephra from the 12–15 August 1991 eruption of Hudson volcano. Bull Volcanol 56(2):121–132. https://doi.org/10.1007/BF00304107

Schumacher R (1994) A reappraisal of Mount St. Helens' ash clusters - depositional model from experimental observation. Journal of Volcanology and Geothermal Research 59(3):253–260. http://www.sciencedirect.com/science/article/pii/037702739490099X

Schumacher R, Schmincke HU (1995) Models for the origin of accretionary lapilli. Bull Volcanol 56(8):626–639. https://doi.org/10.1007/s004450050069

Schuster RL (1981) Effects of the eruptions on civil works and operations in the Pacific Northwest. In: Lipman PW, Mullineaux DR (eds) The 1980 Eruptions of Mount St. Helens, Washington. USGS Professional Paper 1250. U.S. Government Printing Office, Washington, D.C., p 867, https://doi.org/10.3133/pp1250

Schwaiger H, Denlinger R, Mastin LG (2012) Ash3d: a finite-volume, conservative numerical model for ash transport and tephra deposition. Journal of Geophysical Research 117(B04204):doi:https://doi.org/10.1029/2011JB008968. https://doi.org/10.1029/2011JB008968

Searl A, Nicholl A, Baxter PJ (2002) Assessment of the exposure of islanders to ash from the Soufriere Hills volcano, Montserrat, British West Indies. Occup Environ Med 59(8):523–531. https://doi.org/10.1136/oem.59.8.523

Servranckx R, Chen P, Little K (1999) Volcanic ash advisory centers--roles and challenges. In, The 8th Conference on Aviation, Range, and Aerospace Meteorology, https://ams.confex.com/ams/older/99annual/abstracts/960.htm

Settle M (1978) Volcanic eruption clouds and the thermal power output of explosive eruptions. J Volcanol Geoth Res 3:309–324. https://doi.org/10.1016/0377-0273(78)90041-0

Sič B, El Amraoui L, Marécal V, Josse B, Arteta J, Guth J, Joly M, Hamer PD (2015) Modelling of primary aerosols in the chemical transport model MOCAGE: development and evaluation of aerosol physical parameterizations. Geosci. Model Dev. 8(2):381–408. http://www.geosci-model-dev.net/8/381/2015/

Sigurdsson H, Carey SN, Espindola JM (1984) The 1982 eruptions of El Chichón Volcano, Mexico: stratigraphy of pyroclastic deposits. J Volcanol Geoth Res 23(1–2):11–37. https://doi.org/10.1016/0377-0273(84)90055-6

Sisson TW (1995) Blast ashfall deposit of May 18, 1980 at Mount St. Helens, Washington. J Volcanol Geoth Res 66:203–216. https://doi.org/10.1016/0377-0273(94)00063-M

Sorem RK (1982) Volcanic ash clusters: tephra rafts and scavengers. J Volcanol Geoth Res 13:63–71. https://doi.org/10.1016/0377-0273(82)90019-1

Sparks RSJ, Bursik MI, Ablay GJ, Thomas RME, Carey SN (1992) Sedimentation of tephra by volcanic plumes. Part 2: controls on thickness and grain-size variations of tephra fall deposits. Bull Volcanol 54(8):685–695. https://doi.org/10.1007/BF00430779

Sparks RSJ, Bursik MI, Carey SN, Gilbert JS, Glaze LS, Sigurdsson H, Woods AW (1997) Volcanic Plumes. John Wiley & Sons, Chichester, p 574

Sparks RSJ, Huang TC (1980) The volcanological significance of deep-sea ash layers associated with ignimbrites. Geol Mag 117(05):425–436. https://doi.org/10.1017/S0016756800028533

Sparks RSJ, Moore JG, Rice CJ (1986) The initial giant umbrella cloud of the May 18th, 1980, explosive eruption of Mount St. Helens. Journal of Volcanology and Geothermal Research 28(3–4):257–274. https://doi.org/10.1016/0377-0273(86)90026-0

Sparks RSJ, Wilson L (1976) A model for the formation of ignimbrite by gravitational column collapse. J Geol Soc 132(4):441–451. https://doi.org/10.1144/gsjgs.132.4.0441

Stein AF, Draxler RR, Rolph GD, Stunder BJB, Cohen MD, Ngan F (2015) NOAA's HYSPLIT atmospheric transport and dispersion modeling system. Bull Am Meteor Soc 96(12):2059–2077. https://doi.org/10.1175/BAMS-D-14-00110.1

Suzuki T (1983) A theoretical model for dispersion of tephra. In: Shimozuru D, Yokoyama I (eds) Arc Volcanism: Physics and Tectonics. Terra Scientific Publishing Company, Tokyo, pp 95–113

Suzuki YJ, Costa A, Cerminara M, Esposti Ongaro T, Herzog M, Van Eaton AR, Denby LC (2016) Inter-comparison of three-dimensional models of volcanic plumes. J Volcanol Geoth Res 326:26–42. https://doi.org/10.1016/j.jvolgeores.2016.06.011

Telling J, Dufek J (2012) An experimental evaluation of ash aggregation in explosive volcanic eruptions. J Volcanol Geoth Res 209–210:1–8. https://doi.org/10.1016/j.jvolgeores.2011.09.008

Telling J, Dufek J, Shaikh A (2013) Ash aggregation in explosive volcanic eruptions. Geophys Res Lett 40(10):2355–2360. https://doi.org/10.1002/grl.50376

Terry JP, Goff J, Winspear N, Bongolan VP, Fisher S (2022) Tonga volcanic eruption and tsunami, January 2022: globally the most significant opportunity to observe an explosive and tsunamigenic submarine eruption since AD 1883 Krakatau. Geoscience Letters 9(1):24. https://doi.org/10.1186/s40562-022-00232-z

Textor C, Graf HF, Herzog M, Oberhuber JM, Rose WI, Ernst GGJ (2006a) Volcanic particle aggregation in explosive eruption columns. Part I: parameterization of the microphysics of hydrometeors and ash. J Volcanol Geoth Res 150:359–377. https://doi.org/10.1016/j.jvolgeores.2005.09.007

Textor C, Graf HF, Herzog M, Oberhuber JM, Rose WI, Ernst GGJ (2006b) Volcanic particle aggregation in explosive eruption columns. Part II: numerical experiments. Journal of Volcanology and Geothermal Research 150(4):378–394. https://doi.org/10.1016/j.jvolgeores.2005.09.008

Thorsteinsson T, Jóhannsson T, Stohl A, Kristiansen NI (2012) High levels of particulate matter in Iceland due to direct ash emissions by the Eyjafjallajökull eruption and resuspension of deposited ash. Journal of Geophysical Research: Solid Earth 117(B9):n/a-n/a. https://doi.org/10.1029/2011JB008756

Tilling RI (1984) Eruptions of Mount St. Helens: past, present, and future. U.S. Government Printing Office, Washington, D.C., p 56, https://doi.org/10.3133/7000010

Van Eaton AR, Amigo Á, Bertin D, Mastin LG, Giacosa RE, González J, Valderrama O, Fontijn K, Behnke SA (2016) Volcanic lightning and plume behavior reveal evolving hazards during the April 2015 eruption of Calbuco volcano. Chile Geophysical Research Letters 43(7):3563–3571. https://doi.org/10.1002/2016GL068076

Van Eaton AR, Wilson CJN (2013) The nature, origins and distribution of ash aggregates in a large-scale wet eruption deposit: Oruanui, New Zealand. J Volcanol Geoth Res 250:129–154. https://doi.org/10.1016/j.jvolgeores.2012.10.016

Veitch G, Woods AW (2001) Particle aggregation in volcanic eruption columns. J Geophys Res 2001(B11):26,425–426,441. https://doi.org/10.1029/2000JB900343

Voight B (1981) Time scale for the first moments of the May 1981 eruption. In: Lipman PW, Mullineaux DR (eds) The 1980 Eruptions of Mount St. Helens, Washington. USGS Professional Paper 1250. U.S. Government Printing Office, Washington, D.C., pp 69–90, https://doi.org/10.3133/pp1250

Waitt R (2014) In the path of destruction. Washington State University Press, Pullman, Washington

Waitt R, Dzurisin D (1981) proximal air-fall deposits from the May 18 eruption--stratigraphy and field sedimentology. In: Lipman PW, Mullineaux DR (eds) The 1980 Eruptions of Mount St. Helens, Washington. USGS Professional Paper 1250. U.S. Government Printing Office, Washington, D.C., pp 601–615, https://doi.org/10.3133/pp1250

Walker GPL, Wilson L, Bowell ELG (1971) Explosive volcanic eruptions-I the rate of fall of pyroclasts. Geophys J Roy Astron Soc 22(4):377–383. https://doi.org/10.1111/j.1365-246X.1971.tb03607.x

Wallace K, Schwaiger H (2019) Volcanic ash resuspension from the Katmai region. Alaska Park Science 18(1).

Warrick RA, Anderson J, Lyons J, Ressler J, Mary W, Warrick T (1981) Four communities under ash after Mount St. Helens. Program on Technology, Environment, and Man, Monograph #34. Institute of Behavioral Science, University of Colorado, Boulder, CO, p 143,

Webster HN, Devenish BJ, Mastin LG, Thomson DJ, Van Eaton AR (2020) Operational modelling of umbrella cloud growth in a Lagrangian volcanic ash transport and dispersion model. Atmosphere 11(2):200. https://doi.org/10.3390/atmos11020200

Wiesner M, Wetzel A, Catane S, Listanco E, Mirabueno H (2004) Grain size, areal thickness distribution and controls on sedimentation of the 1991 Mount Pinatubo tephra layer in the South China Sea. Bull Volcanol 66(3):226–242. https://doi.org/10.1007/s00445-003-0306-x

Wilson CJN (2001) The 26.5ka Oruanui eruption, New Zealand: an introduction and overview. Journal of Volcanology and Geothermal Research 112(1–4):133–174. https://doi.org/10.1016/S0377-0273(01)00239-6

Wilson L (1972) Explosive volcanic eruptions-II the atmospheric trajectories of pyroclasts. Geophys J Roy Astron Soc 30(4):381–392. https://doi.org/10.1111/j.1365-246X.1972.tb05822.x

Wilson L (1976) Explosive volcanic eruptions III, Plinian eruption columns. Geophys J Roy Astron Soc 45:543–556. https://doi.org/10.1111/j.1365-246X.1958.tb05342.x

Wilson L, Sparks RSJ, Huang TC, Watkins ND (1978) The control of volcanic column heights by eruption energetics and dynamics. J Geophys Res 83(B4):1829–1836. https://doi.org/10.1029/JB083iB04p01829

Wilson TM, Jenkins S, Stewart C (2015) Impacts from volcanic ash fall. In: Papale P (ed) Volcanic Hazards, Risks, and Disasters. Elsevier, Dordrecht, pp 47–86, https://doi.org/10.1016/B978-0-12-396453-3.00003-4

Woods AW, Holasek RE, Self S (1995) Wind-driven dispersal of volcanic ash plumes and its control on the thermal structure of the plume-top. Bull Volcanol 57(5):283–292. https://doi.org/10.1007/BF00301288

Woods AW, Self S (1992) Thermal disequilibrium at the top of volcanic clouds and its effect on estimates of the column height. Nature 355(6361):628–630. https://doi.org/10.1038/355628a0

Woods AW, Wohletz K (1991) Dimensions and dynamics of co-ignimbrite eruption columns. Nature 350(6315):225–227. https://doi.org/10.1038/350225a0